

1 Identification of dominant hydrogeochemical processes for  
2 groundwaters in Algerian Sahara supported by inverse modeling  
3 of chemical and isotopic data

4 R. Slimani<sup>a</sup>, A. Guendouz<sup>b</sup>, F. Trolard<sup>c</sup>, A.S. Moulla<sup>d</sup>, B. Hamdi-Aïssa<sup>a</sup>, G. Bourrié<sup>c</sup>

5 <sup>a</sup>*Ouargla University, Fac. des Sciences de la Nature et de la Vie, Lab. Biochimie des Milieux Désertiques, Ouargla*  
6 *30000, Algeria*

7 <sup>b</sup>*Blida University, Science and Engineering Faculty, P.O.Box 270 Soumaa, Blida, Algeria*

8 <sup>c</sup>*INRA, UMR 1114 Emmah, Avignon, France*

9 <sup>d</sup>*Algiers Nuclear Research Centre, P.O. Box, 399 Alger-RP, 16000 Algiers, Algeria*

---

10 **Abstract**

Unpublished chemical and isotopic data taken in November 1992 from the three major Saharan aquifers namely, the “Continental Intercalaire” (CI), the “Complexe Terminal” (CT) and the Phreatic aquifer (Phr) were integrated with original samples in order to chemically and isotopically characterize a Saharan aquifer system and investigate the processes through which groundwaters acquire their mineralization. Instead of classical Debye-Hückel extended law, Specific Interaction Theory (SIT) model, recently incorporated in Phreeqc 3.0 was used. Inverse modeling of hydrochemical data constrained by isotopic data was used here to quantitatively assess the influence of geochemical processes: at depth, the dissolution of salts from the geological formations during upward leakage without evaporation explains the transitions from CI to CT and to a first end member, cluster of Phr (cluster I); near the surface, the dissolution of salts from sebkhas by rainwater explains another cluster of Phr (cluster II). In every case, secondary precipitation of calcite occurs during dissolution. All Phr waters result from the mixing of these two clusters together with calcite precipitation and ion exchange processes. These processes are quantitatively assessed by Phreeqc model. Globally, gypsum dissolution and calcite precipitation were found to act as a carbon sink.

11 *Keywords:* hydrochemistry, stable isotopes, Sahara, Algeria

---

12 **1. INTRODUCTION**

13 A scientific study published in 2008 (OECD, 2008) showed that 85% of the world population  
14 lives in the driest half of the Earth. More than 1 billion people residing in arid and semi-arid areas  
15 of the world have only access to little or no renewable water resources. In many arid regions such  
16 as Sahara, groundwater is the only source of water supply for domestic, agricultural or industrial  
17 purposes, often causing overuse and / or degradation of water quality.

18 The groundwater resources of Ouargla basin (Lower-Sahara, Algerian) (Fig. 1) are contained  
19 in three main reservoirs (UNESCO, 1972; Eckstein and Eckstein, 2003; OSS, 2003, 2008):

---

*Email address:* [slm\\_rabia@yahoo.fr](mailto:slm_rabia@yahoo.fr) (R. Slimani)

- 20 • at the top, the phreatic aquifer (Phr), located in sandy gypsum permeable formations of  
21 Quaternary, is almost unexploited, due to its salinity (50 g/L);
- 22 • in the middle, the “Complexe Terminal” (CT) (Cornet and Gouscov, 1952; UNESCO,  
23 1972) is the most exploited and includes several aquifers in different geological forma-  
24 tions. Groundwater circulates in one or two lithostratigraphic formations of the Eocene  
25 and Senonian carbonates or Mio-pliocene sands;
- 26 • at the bottom, the “Continental Intercalaire” (CI), hosted in the lower Cretaceous continen-  
27 tal formations (Barremian and Albian), mainly composed of sandstones, sands and clays.  
28 It is only partially exploited because of its significant depth.

29 After use, waters are discharged in a closed system (endorheic basin) and constitute a po-  
30 tential hazard to the environment, to public health and may jeopardize the sustainability of agri-  
31 culture, due to rising of the phreatic aquifer watertable, extension of soil salinization and so  
32 on (Hamdi-Aïssa et al., 2004; Slimani, 2006). Several studies (Guendouz, 1985; Fontes et al.,  
33 1986; Guendouz and Moulla, 1996; Edmunds et al., 2003; Guendouz et al., 2003; Hamdi-Aïssa  
34 et al., 2004; Foster et al., 2006; OSS, 2008; Al-Gamal, 2011) started from chemical and isotopic  
35 information ( $^2\text{H}$ ,  $^{18}\text{O}$ ,  $^{234}\text{U}$ ,  $^{238}\text{U}$ ,  $^{36}\text{Cl}$ ) to characterize the relationships between aquifers. In  
36 particular, such studies focused on the recharge of the deep CI aquifer system. These investi-  
37 gations dealt particularly with water chemical facies, mapped isocontents of various parameters,  
38 and reported typical geochemical ratios ( $[\text{SO}_4^{2-}]/[\text{Cl}^-]$ ,  $[\text{Mg}^{2+}]/[\text{Ca}^{2+}]$ ) as well as other correla-  
39 tions. Minerals / solutions equilibria were checked by computing saturation indices with respect  
40 to calcite, gypsum, anhydrite and halite, but processes were only qualitatively assessed.

41 The present study aims at applying for the first time ever in Algeria, inverse modeling to an  
42 extreme environment, characterized by a lack of data on a scarce natural resource (groundwater).  
43 In the present study, new data were collected in order to characterize the hydrochemical and  
44 the isotopic composition of the major aquifers in Ouargla’s region and identify the origin of the  
45 mineralization and water-rock interactions that occur along the flow. New possibilities offered  
46 by progress in geochemical simulations were used. More specifically, evaporite dissolution, ion  
47 exchange, calcite dissolution / precipitation and  $\text{CO}_2$  escape or dissolution and mixing can be  
48 quantitatively assessed by inverse modeling (Dai et al., 2006) with Phreeqc 3.0 to explain the  
49 modifications of the chemical composition of the three main Saharan aquifers. This results in  
50 constraints on mass balances as well as on the exchange of matter between aquifers.

## 51 2. METHODOLOGY

### 52 2.1. Presentation of the study area

53 The study area is located in the northeastern desert of Algeria “Lower-Sahara” (Le Houérou,  
54 2009) near the city of Ouargla (Fig. 1),  $31^\circ 54'$  to  $32^\circ 1' \text{ N}$  and  $5^\circ 15'$  to  $5^\circ 27' \text{ E}$ , with a mean ele-  
55 vation of 134 (m.a.s.l.). It is located in the quaternary valley of Oued Mya basin. Present climate  
56 belongs to the arid Mediterranean-type (Dubief, 1963; Le Houérou, 2009; ONM, 1975/2013), as  
57 it is characterized by a mean annual temperature of  $22.5^\circ\text{C}$ , a yearly rainfall of 43.6 mm/yr and  
58 a very high evaporation rate of 2,138 mm/yr.

59 Ouargla’s region and the entire Lower Sahara has experienced during its long geological history  
60 alternating marine and continental sedimentation phases. During Secondary era, vertical move-  
61 ments affected the Precambrian basement causing in particular collapse of its central part, along

62 an axis passing approximately through the Oued Righ valley and the upper portion of the val-  
63 ley oued Mya. According to Furon (1960), an epicontinental sea spread to the Lower Eocene of  
64 northern Sahara. After the Oligocene, the sea gradually withdrew. It is estimated at present that  
65 this sea did not reach Ouargla and transgression stopped at the edge of the bowl (Furon, 1960;  
66 Lelièvre, 1969). The basin is carved into Mio-pliocene (MP) deposits, which alternate with red  
67 sands, clays and sometimes marls; gypsum is not abundant and dated from Pontian (MP) (Cornet  
68 and Gouscov, 1952; Dubief, 1953; Ould Baba Sy and Besbes, 2006). The continental Pliocene  
69 consists of a local limestone crust with puddingstone or lacustrine limestone (Fig. 2), shaped  
70 by eolian erosion into flat areas (regs). The Quaternary formations are lithologically composed  
71 of alternating layers of permeable sand and relatively impermeable marl (Aumassip et al., 1972;  
72 Chellat et al., 2014).

73 The exploitation of Mio-pliocene aquifer is ancient and at the origin of the creation of the  
74 oasis (Lelièvre, 1969; Moulias, 1927). The piezometric level was higher (145 m a.s.l.) but over-  
75 exploitation at the end of the XIXth century led to a catastrophic decrease of the resource, with  
76 presently more than 900 boreholes (ANRH, 2011).

77 The exploitation of Senonian aquifer dates back to 1953 at a depth between 140 to 200 m,  
78 with a small initial rate *ca.*  $9 \text{ L s}^{-1}$ ; two boreholes have been exploited since 1965 and 1969, with  
79 a total flowrate *ca.*  $42 \text{ L s}^{-1}$ , for drinking water and irrigation.

80 The exploitation of Albian aquifer dates back to 1956, presently, two boreholes are exploited:

- 81 • El Hedeb I, 1,335 m deep, with a flowrate  $141 \text{ L s}^{-1}$ ;
- 82 • El Hedeb II, 1,400 m deep, with a flowrate  $68 \text{ L s}^{-1}$ .

## 83 2.2. Sampling and analytical methods

84 The sampling programme consisted of collecting samples along transects corresponding to  
85 directions of flow for both Phr and CT aquifers while it was possible to collect only eight samples  
86 from the CI. A total of 107 samples were collected during a field campaign in 2013, along the  
87 main flowpath of Oued Mya. 67 of them were from piezometers tapping the phreatic aquifer,  
88 32 from CT wells and the last 8 from boreholes tapping the CI aquifer (Fig. 3). Analyses of  
89  $\text{Na}^+$ ,  $\text{K}^+$ ,  $\text{Ca}^{2+}$ ,  $\text{Mg}^{2+}$ ,  $\text{Cl}^-$ ,  $\text{SO}_4^{2-}$  and  $\text{HCO}_3^-$  were performed by ion chromatography at Algiers  
90 Nuclear Research Center (CRNA). Previous and yet unpublished data (Guendouz and Moulla,  
91 1996) sampled in 1992 are used here too: 59 samples for Phr aquifer, 15 samples for CT aquifer  
92 and 3 samples for the CI aquifer for chemical analyses, data  $^{18}\text{O}$  and  $^3\text{H}$  (Guendouz and Moulla,  
93 1996).

## 94 2.3. Geochemical method

95 Phreeqc was used to check minerals / solution equilibria using the specific interaction the-  
96 ory (SIT), *i.e.* the extension of Debye-Hückel law by Scatchard and Guggenheim incorporated  
97 recently in Phreeqc 3.0 (Parkhurst and Appelo, 2013). Inverse modeling was used to calculate  
98 the number of minerals and gases' moles that must respectively dissolve or precipitate/degas to  
99 account for the difference in composition between initial and final water end members (Plum-  
100 mer and Back, 1980; Kenoyer and Bowser, 1992; Deutsch, 1997; Plummer and Sprinkle, 2001;  
101 Güler and Thyne, 2004; Parkhurst and Appelo, 2013). This mass balance technique has been  
102 used to quantify reactions controlling water chemistry along flow paths (Thomas et al., 1989).  
103 It is also used to quantify the mixing proportions of end-member components in a flow system  
104 (Kuells et al., 2000; Belkhiri et al., 2010, 2012).

105 Inverse modeling involves designing a list of scenarios (modelling setups) that take into account  
106 the most plausible combinations of geochemical processes that are likely to occur in our  
107 system. For example, the way to identify whether calcite dissolution/precipitation is relevant or  
108 not consists of solving the inverse problem under two alternate scenarios: (1) considering a geo-  
109 chemical system in which calcite is present, and (2) considering a geochemical system without  
110 calcite. After simulating the two scenarios, it is usually possible to select the setup that gives the  
111 best results as the solution to the inverse modeling according to the fit between the modeled and  
112 observed values. Then one can conclude whether calcite dissolution/precipitation is relevant or  
113 not. This stepwise strategy allows us to identify the relevance of a given chemical process by  
114 inversely solving the problem through alternate scenarios in which the process is either partici-  
115 pating or not.

### 116 3. RESULTS AND DISCUSSION

117 Tables 1 to 4 illustrate the results of the chemical and the isotopic analyses. Samples are  
118 ordered according to an increasing electric conductivity (EC), and this is assumed to provide  
119 an ordering for increasing salt content. In both phreatic and CT aquifers, temperature is close to  
120 25 °C, while for CI aquifer, temperature is close to 50 °C. The values presented in tables 1 to 5 are  
121 raw analytical data that were corrected for defects of charge balance before computing activities  
122 with Phreeqc. As analytical errors could not be ascribed to a specific analyte, the correction was  
123 made proportionally. The corrections do not affect the anions to anions mole ratios such as for  
124  $[\text{HCO}_3^-]/([\text{Cl}^-] + 2[\text{SO}_4^{2-}])$  or  $[\text{SO}_4^{2-}]/[\text{Cl}^-]$ , whereas they affect the cation to anion ratio such  
125 as for  $[\text{Na}^+]/[\text{Cl}^-]$ .

#### 126 3.1. Characterization of chemical facies of the groundwater

127 Piper diagrams drawn for the studied groundwaters (Fig. 4) broadly show a scatter plot domi-  
128 nated by a Chloride-Sodium facies. However, when going into small details, the widespread  
129 chemical facies of the Phr aquifer is closer to the NaCl cluster than those of CI and CT aquifers.  
130 Respectively,  $\text{CaSO}_4$ ,  $\text{Na}_2\text{SO}_4$ ,  $\text{MgSO}_4$  and NaCl are the most dominant chemical species (miner-  
131 als) that are present in the phreatic waters. This sequential order of solutes is comparable to  
132 that of other groundwater occurring in North Africa, and especially in the neighboring area of  
133 the chotts (depressions where salts concentrate by evaporation) Merouane and Melrhir (Vallès  
134 et al., 1997; Hamdi-Aïssa et al., 2004).

#### 135 3.2. Spatial distribution of the mineralization

136 The salinity of the phreatic aquifer varies considerably depending on the location (namely,  
137 the distance from wells or drains) and time (due to the influence of irrigation) (Fig. 5a).

138 Its salinity is low around irrigated and fairly well-drained areas, such as the palm groves of  
139 Hassi Miloud, just north of Ouargla (Fig. 3) that benefit from freshwater and are drained to the  
140 sebkha Oum el Raneb. However, the three lowest salinity values are observed in the wells of  
141 Ouargla palm-grove itself, where the Phr aquifer watertable is deeper than 2 m.

142 Conversely, the highest salinity waters are found in wells drilled in the chotts and sebkhas (a  
143 sebkha is the central part of a chott where salinity is the largest) (Safioune and Oum er Raneb)  
144 where the aquifer is often shallower than 50 cm.

145 The salinity of the CT (Mio-pliocene) aquifer (Fig. 5b) is much lower than that of the Phr  
146 aquifer, and ranges from 1 to 2 g/L; however, its hardness is larger and it contains more sulfate,

147 chloride and sodium than the waters of the Senonian formations and those of the CI aquifer. The  
148 salinity of the Senonian aquifer ranges from 1.1 to 1.7 g/L, while the average salinity of the CI  
149 aquifer is 0.7 g/L (Fig. 5c).

150 A likely contamination of the Mio-pliocene aquifer by phreatic groundwaters through casing  
151 leakage in an area where water is heavily loaded with salt and therefore particularly aggressive  
152 cannot be excluded.

### 153 3.3. Saturation Indices

154 The calculated saturation indices (SI) reveal that waters from CI at 50 °C are close to equi-  
155 librium with respect to calcite, except for 3 samples that are slightly oversaturated. They are  
156 however all undersaturated with respect to gypsum (Fig. 6).

157 Moreover, they are oversaturated with respect to dolomite and undersaturated with respect to  
158 anhydrite and halite (Fig. 7).

159 Waters from CT and phreatic aquifers show the same pattern, but some of them are more  
160 largely oversaturated with respect to calcite, at 25 °C.

161 However, several phreatic waters (P031, P566, PLX4, PL18, P002, P023, P116, P066, P162  
162 and P036) that are located in the sebkhas of Sefioune, Oum-er-Raneb, Bamendil and Ain el  
163 Beida's chott are saturated with gypsum and anhydrite. This is in accordance with highly evapo-  
164 rative environments found elsewhere (UNESCO, 1972; Hamdi-Aïssa et al., 2004; Slimani, 2006).

165 No significant trend of SI from south to north upstream and downstream of Oued Mya (Fig. 7)  
166 is observed. This suggests that the acquisition of mineralization is due to geochemical processes  
167 that have already reached equilibrium or steady state in the upstream areas of Ouargla.

### 168 3.4. Change of facies from the carbonated cluster to the evaporites' cluster

169 The facies shifts progressively from the carbonated (CI and CT aquifers) to the evaporites'  
170 one (Phr aquifer) with an increase in sulfates and chlorides at the expense of carbonates (SI  
171 of gypsum, anhydrite and halite). This is illustrated by a decrease of the  $[\text{HCO}_3^-]/([\text{Cl}^-] +$   
172  $2[\text{SO}_4^{2-}])$  ratio (Fig. 8) from 0.2 to 0 and of the  $[\text{SO}_4^{2-}]/[\text{Cl}^-]$  ratio from 0.8 to values smaller  
173 than 0.3 (Fig. 9) while salinity increases. Carbonate concentrations tend towards very small  
174 values, while it is not the case for sulfates. This is due to both gypsum dissolution and calcite  
175 precipitation.

176 Chlorides in groundwater may come from three different sources: (i) ancient sea water en-  
177 trapped in sediments; (ii) dissolution of halite and related minerals that are present in evaporite  
178 deposits and (iii) dissolution of dry fallout from the atmosphere, particularly in these arid regions  
179 (Matiatos et al., 2014; Hadj-Ammar et al., 2014).

180  $[\text{Na}^+]/[\text{Cl}^-]$  ratio ranges from 0.85 to 1.26 for CI aquifer, from 0.40 to 1.02 for the CT aquifer,  
181 from 0.13 to 2.15 for the Phr aquifer. The measured points from the three considered aquifers  
182 are linearly scattered with good approximation around the unity slope straight line that stands  
183 for halite dissolution (Fig. 10). The latter appears as the most dominant reaction occurring in  
184 the medium. However, at very high salinity,  $\text{Na}^+$  seems to swerve from the straight line, towards  
185 smaller values.

186 A further scrutiny of Fig. 10 shows that CI waters are very close to the 1:1 line. CT waters  
187 are enriched in both  $\text{Na}^+$  and  $\text{Cl}^-$  but slightly lower than the 1:1 line while phreatic waters are  
188 largely enriched and much more scattered. CT waters are closer to the seawater mole ratio  
189 (0.858), but some lower values imply a contribution from another source of chloride than halite  
190 or from entrapped seawater. Conversely, a  $[\text{Na}^+]/[\text{Cl}^-]$  ratio larger than 1 is observed for phreatic

191 waters, which implies the contribution of another source of sodium, most likely sodium sulfate,  
192 that is present as mirabilite or thenardite in the chotts and the sebkhas areas.

193  $[\text{Br}^-]/[\text{Cl}^-]$  ratio ranges from  $2 \times 10^{-3}$  to  $3 \times 10^{-3}$ . The value of this molar ratio for halite is  
194 around  $2.5 \times 10^{-3}$ , which matches the aforementioned range and confirms that halite dissolution  
195 is the most dominant reaction taking place in the studied medium.

196 In the CI, CT and Phr aquifers, calcium originates both from carbonate and sulfate (Fig. 11  
197 and 12). Three samples from CI aquifer are close to the  $[\text{Ca}^{2+}]/[\text{HCO}_3^-]$  1:2 line, while calcium  
198 sulfate dissolution explains the excess of calcium. However, nine samples from Phr aquifer are  
199 depleted in calcium, and plot under the  $[\text{Ca}^{2+}]/[\text{HCO}_3^-]$  1:2 line. This cannot be explained by  
200 precipitation of calcite, as some are undersaturated with respect to that mineral, while others are  
201 oversaturated.

202 In this case, a cation exchange process seems to occur and lead to a preferential adsorption  
203 of divalent cations, with a release of  $\text{Na}^+$ . This is confirmed by the inverse modeling that is  
204 developed below and which implies  $\text{Mg}^{2+}$  fixation and  $\text{Na}^+$  and  $\text{K}^+$  releases.

205 Larger sulfate values observed in the phreatic aquifer (Fig. 12) with  $[\text{Ca}^{2+}]/[\text{SO}_4^{2-}] < 1$  can  
206 be attributed to a Na-Mg sulfate dissolution from a mineral bearing such elements. This is for  
207 instance the case of bloedite.

208

### 209 3.5. Isotope geochemistry

210 CT and CI aquifer exhibit depleted and homogeneous  $^{18}\text{O}$  contents, ranging from  $-8.32\text{‰}$   
211 to  $-7.85\text{‰}$ . This was already previously reported by many authors (Edmunds et al., 2003;  
212 Guendouz et al., 2003; Moulla et al., 2012). On the other hand,  $^{18}\text{O}$  values for the phreatic  
213 aquifer are widely dispersed and vary between  $-8.84\text{‰}$  to  $3.42\text{‰}$  (Table 5). Waters located  
214 north of the virtual line connecting approximately Hassi-Miloud to sebkhet Safioune, are found  
215 more enriched in heavy isotopes and are thus more evaporated. In that area, water table is close to  
216 the surface and mixing of both CI and CT groundwaters with phreatic ones through irrigation is  
217 nonexistent. Conversely, waters located south of Hassi Miloud up to Ouargla city show depleted  
218 values. This is the clear fingerprint of a contribution to the Phr waters from the underlying CI  
219 and CT aquifers (Gonfiantini et al., 1975; Guendouz, 1985; Fontes et al., 1986; Guendouz and  
220 Moulla, 1996).

221 Phreatic waters result from a mixing of two end-members. An evidence for this is given by  
222 considering the  $([\text{Cl}^-], ^{18}\text{O})$  relationship (Fig. 13). The two clusters are: i) a first cluster of  $^{18}\text{O}$   
223 depleted groundwater (Fig. 14), and ii) another cluster of  $^{18}\text{O}$  enriched groundwater with positive  
224 values and a high salinity. The latter is composed of phreatic waters occurring in the northern  
225 part of the study region.

226 Cluster I represents the waters from CI and CT whose isotopic composition is depleted  
227 in  $^{18}\text{O}$  (average value around  $-8.2\text{‰}$ ) (Fig. 13). They correspond to an old water recharge  
228 (palæorecharge); whose age estimated by means of  $^{14}\text{C}$ , exceeds 15.000 years BP (Guendouz,  
229 1985; Guendouz and Michelot, 2006). So, it is not a water body that is recharged by recent  
230 precipitation. It consists of CI and CT groundwaters and partly of phreatic waters, and can be  
231 ascribed to an upward leakage favored by the extension of faults near Amguid El-Biod dorsal.

232 Cluster II, observed in Sebkhet Safioune, can be ascribed to the direct dissolution of surficial  
233 evaporitic deposits conveyed by evaporated rainwater.

234 Evaporation alone cannot explain the distribution of data that is observed (Fig. 13). An  
235 evidence for this is given in a semi-logarithmic plot (Fig. 14), as classically obtained according  
236 to the simple approximation of Rayleigh equation (cf. Appendix):

$$\delta^{18}\text{O} \approx 1000 \times (1 - \alpha) \log[\text{Cl}^-] + k, \quad (1)$$

$$\approx -\epsilon \log[\text{Cl}^-] + k, \quad (2)$$

237 where  $\alpha$  is the fractionation factor during evaporation,  $\epsilon \equiv -1000 \times (1 - \alpha)$  is the enrichment  
238 factor and  $k$  is a constant (Ma et al., 2010; Chkir et al., 2009).

239 CI and CT waters are better separated in the semi-logarithmic plot because they are differen-  
240 tiated by their chloride content. According to equation (1), simple evaporation gives a straight  
241 line (solid line in Fig. 14). The value of  $\epsilon$  used is the value at 25 °C, which is equal to  $-73.5$ .

242 P115 is the only sample that appears on the straight evaporation line (Fig. 14). It should be  
243 considered as an outlier since the rest of the samples are all well aligned on the logarithmic fit  
244 derived from the mixing line of Figure 13.

245 The phreatic waters that are close to cluster I (Fig. 13) correspond to groundwaters occur-  
246 ring in the edges of the basin (Hassi Miloud, piezometer P433) (Fig. 14). They are low-  
247 mineralized and acquire their salinity via two processes, namely: dissolution of evaporites along  
248 their underground transit up to Sebkheth Safioune and dilution through upward leakage by the  
249 less-mineralized waters of CI and CT aquifers (for example Hedeb I for CI and D7F4 for CT)  
250 (Fig. 14) (Guendouz, 1985; Guendouz and Moulla, 1996).

251 The rates of the mixing that are due to upward leakage from CI to CT towards the phreatic  
252 aquifer can be calculated by means of a mass balance equation. It only requires knowing the  $\delta$   
253 values of each fraction that is involved in the mixing process.

254 The  $\delta$  value of the mixture is given by:

$$\delta_{\text{mix}} = f \times \delta_1 + (1 - f) \times \delta_2 \quad (3)$$

255 where  $f$  is the fraction of CI aquifer,  $1 - f$  the fraction of the CT and  $\delta_1$ ,  $\delta_2$  are the respective  
256 isotope contents.

257 Average values of mixing fractions from each aquifer to the phreatic waters computed by  
258 means of equation (3) gave the rates of 65 % for CI aquifer and 35% for CT aquifer.

259 A mixture of a phreatic water component that is close to cluster I (*i.e.* P433) with another  
260 component which is rather close to cluster II (*i.e.* P039) (Fig. 13 and 14), for an intermediate  
261 water with a  $\delta^{18}\text{O}$  signature ranging from  $-5 \text{‰}$  to  $-2 \text{‰}$  gives mixture fraction values of 52 %  
262 for cluster I and 48 % for cluster II. Isotope results will be used to independently cross-check the  
263 validity of the mixing fractions derived from an inverse modeling involving chemical data (see  
264 section 3.6).

265 Turonian evaporites are found to lie in between CI deep aquifer and the Senonian and Miocene  
266 formations bearing CT aquifer. CT waters can thus simply originate from ascending CI waters  
267 that dissolve Turonian evaporites, a process which does not involve any change in  $^{18}\text{O}$  content.  
268 Conversely, phreatic waters result to a minor degree from evaporation and mostly from dissolu-  
269 tion of sebkhas evaporites by  $^{18}\text{O}$  enriched rainwater and mixing with CI-CT waters.

### 270 3.5.1. Tritium content of water

271 Tritium contents of Phr aquifer are relatively small (Table 5), they vary between 0 and 8 TU.  
272 Piezometers PZ12, P036 and P068 show values close to 8 TU, piezometers P018, P019, P416,  
273 P034, P042 and P093 exhibit values ranging between 5 and 6 TU, and the rest of the samples'  
274 concentrations are lower than 2 TU.

275 These values are dated back to November 1992 so they are old values and they are considered  
276 high comparatively to what is expected to be found nowadays. In fact, at present times, tritium  
277 figures have fallen lower than 5 TU in precipitation measured in the northern part of the country.

278 Tritium content of precipitation was measured as 16 TU in 1992 on a single sample that was  
279 collected from the National Agency for Water Resources station in Ouargla. A major part of  
280 this rainfall evaporates back into the atmosphere that is unsaturated in moisture. Consequently,  
281 enrichment in tritium happens as water evaporates back.

282 The lightest fractions (isotopes) are the ones that escape first causing enriching the remaining  
283 fraction in tritium. The 16 TU value would thus correspond to a rainy event that had happened  
284 during the field campaign (5, 6 Nov. 1992). It is the most representative value for that region  
285 and for that time. Unfortunately, all the other stations (Algiers, Ankara, and Tenerife) (Martinelli  
286 et al., 2014) are subject to a completely different climatic regime and besides the fact that they  
287 have more recent values, can absolutely not be used for our case. Therefore all the assumptions  
288 based on recent tritium rain values do not apply to this study.

289 Depleted contents in  $^{18}\text{O}$  and low tritium concentrations for phreatic waters fit well the mix-  
290 ing scheme and confirm the contribution from the older and deeper CI/CT groundwaters. The  
291 affected areas were clearly identified in the field and correspond to locations that are subject to  
292 a recycling and a return of irrigation waters whose origin are CI/CT boreholes. Moreover, the  
293 mixing that is clearly brought to light by the  $\text{Cl}^-$  vs.  $^{18}\text{O}$  diagrams (Fig. 13 and 14) could partly  
294 derive from an ascending drainage from the deep and confined CI aquifer (exhibiting depleted ho-  
295 mogenous  $^{18}\text{O}$  contents and very low tritium), a vertical leakage that is favoured by the Amguid  
296 El-biod highly faulted area (Guendouz and Moulla, 1996; Edmunds et al., 2003; Guendouz et al.,  
297 2003; Moulla et al., 2012).

### 298 3.6. Inverse modeling

299 We assume that the relationship between  $^{18}\text{O}$  and  $\text{Cl}^-$  data obtained in 1992 is stable with  
300 time, which is a logical assumption as times of transfer from CI to both CT and Phr are very long.  
301 Considering both  $^{18}\text{O}$  and  $\text{Cl}^-$  data, CI, CT and Phr data populations can be categorized. The CI  
302 and CT do not show appreciable  $^{18}\text{O}$  variations, and can be considered as a single population. The  
303 Phr samples consist however of different populations: cluster I, with  $\delta^{18}\text{O}$  values close to -8, and  
304 small  $\text{Cl}^-$  concentrations, more specifically less than  $35 \text{ mmol L}^{-1}$ ; cluster II, with  $\delta^{18}\text{O}$  values  
305 larger than 3, and very large  $\text{Cl}^-$  concentrations, more specifically larger than  $4,000 \text{ mmol L}^{-1}$   
306 (Table 6); intermediate Phr samples result from mixing between clusters I and II (mixing line in  
307 Fig. 13, mixing curve in Fig. 14) and from evaporation of cluster I (evaporation line in Fig. 14).

308 The mass-balance modeling has shown that relatively few phases are required to derive ob-  
309 served changes in water chemistry and to account for the hydrochemical evolution in Ouargla's  
310 region. The mineral phases' selection is based upon geological descriptions and analysis of rocks  
311 and sediments from the area (OSS, 2003; Hamdi-Aïssa et al., 2004).

312 The inverse model was constrained so that mineral phases from evaporites including gypsum,  
313 halite, mirabilite, glauberite, sylvite and bloedite were set to dissolve until they reach saturation,  
314 and calcite, dolomite were set to precipitate once they reached saturation. Cation exchange reac-  
315 tions of  $\text{Ca}^{2+}$ ,  $\text{Mg}^{2+}$ ,  $\text{K}^+$  and  $\text{Na}^+$  on exchange sites were included in the model to check which  
316 cations are adsorbed or desorbed during the process. Dissolution and desorption contribute as  
317 positive terms in the mass balance, as elements are released in solution. On the other hand,  
318 precipitation and adsorption contribute as negative terms, while elements removed from the so-  
319 lution.  $\text{CO}_{2(\text{g})}$  dissolution is considered by Phreeqc as a dissolution of a mineral, whereas  $\text{CO}_{2(\text{g})}$   
320 degassing is dealt with as if it were a mineral precipitation.



321 Inverse modelling leads to a quantitative assessment of the different solutes' acquisition pro-  
322 cesses and a mass balance for the salts that are dissolved or precipitated from CI, CT and Phr  
323 groundwaters (Fig. 14, Table 7), as follows:

- 324 • transition from CI to CT involves gypsum, halite and sylvite dissolution, and some ion  
325 exchange namely calcium and potassium fixation on exchange sites against magnesium  
326 release, with a very small and quite negligible amount of  $\text{CO}_{2(g)}$  degassing. The maximum  
327 elemental concentration fractional error equals 1%. The model consists of a minimum  
328 number of phases (*i.e.* 6 solid phases and  $\text{CO}_{2(g)}$ ); Another model implies as well dolomite  
329 precipitation with the same fractional error;
- 330 • transition from CT to an average water component of cluster I involves dissolution of  
331 halite, sylvite, and bloedite from Turonian evaporites, with a very tiny calcite precipitation.  
332 The maximum fractional error in elemental concentration is 4%. Another model implies  
333  $\text{CO}_{2(g)}$  escape from the solution, with the same fractional error. Large amounts of  $\text{Mg}^{2+}$   
334 and  $\text{SO}_4^{2-}$  are released within the solution (Sharif et al., 2008; Li et al., 2010; Carucci  
335 et al., 2012);
- 336 • the formation of Phr cluster II can be modeled as being a direct dissolution of salts from the  
337 sebkha by rainwater with positive  $\delta^{18}\text{O}$ ; the most concentrated water (P036 from Sebket  
338 Safioune) is taken here for cluster II, and pure water as rainwater. In a descending order  
339 of amount, halite, sylvite, gypsum and huntite are the minerals that are the most involved  
340 in the dissolution process. A small amount of calcite precipitates while some  $\text{Mg}^{2+}$  are  
341 released versus  $\text{K}^+$  fixation on exchange sites. The maximum elemental fractional error in  
342 the concentration is equal to 0.004%. Another model implies dolomite precipitation with  
343 some more huntite dissolving, instead of calcite precipitation, but salt dissolution and ion  
344 exchange are the same. Huntite, dolomite and calcite stoichiometries are linearly related,  
345 so both models can fit field data, but calcite precipitation is preferred compared to dolomite  
346 precipitation at low temperature;
- 347 • the origin of all phreatic waters can be explained by a mixing in variable proportions  
348 of cluster I and cluster II. For instance, waters from cluster I and cluster II can easily be  
349 separated by their  $\delta^{18}\text{O}$  respectively close to  $-8\text{‰}$  and  $3.5\text{‰}$  (Fig. 13 and 14). Mixing the  
350 two clusters is of course not an inert reaction, but rather results in the dissolution and the  
351 precipitation of minerals. Inverse modeling is then used to compute both mixing rates and  
352 the extent of matter exchange between soil and solution. For example, a phreatic water  
353 (piezometer P068) with intermediate values ( $\delta^{18}\text{O} = -3$  and  $[\text{Cl}^-] \simeq 2\text{ M}$ ) is explained  
354 by the mixing of 58% water from cluster I and 42% from cluster II. In addition, calcite  
355 precipitates,  $\text{Mg}^{2+}$  fixes on exchange sites, against  $\text{Na}^+$  and  $\text{K}^+$ , gypsum dissolves as well  
356 as a minor amount of huntite (Table 7). The maximum elemental concentration fractional  
357 error is 2.5% and the mixing fractions' weighted the  $\delta^{18}\text{O}$  is  $-3.17\text{‰}$ , which is very  
358 close to the measured value ( $-3.04\text{‰}$ ). All the other models, making use of a minimum  
359 number of phases, and not taking into consideration ion exchange reactions are not found  
360 compatible with isotope data. Mixing rates obtained with such models are for example  
361 98% of cluster I and 0.9% of cluster II, which leads to a  $\delta^{18}\text{O} = (-7.80\text{‰})$  which is quite  
362 far for the real measured value ( $-3.04\text{‰}$ ).

363 The main types of groundwaters occurring in Ouargla basin are thus explained and could  
364 quantitatively be reconstructed. An exception is however sample P115, which is located exactly

365 on the evaporation line of Phr cluster I. Despite numerous attempts, it could not be quantitatively  
366 rebuilt. Its  $^3\text{H}$  value (6.8) indicates that it is derived from a more or less recent water component  
367 with very small salt content, most possibly affected by rainwater and some preferential flow  
368 within the piezometer. As this is the only sample on this evaporation line, there remains a doubt  
369 on its significance.

370 Globally, the summary of mass transfer reactions occurring in the studied system (Table 7)  
371 shows that gypsum dissolution results in calcite precipitation and  $\text{CO}_{2(\text{g})}$  dissolution, thus acting  
372 as an inorganic carbon sink.

#### 373 4. CONCLUSIONS

374 From the three aquifers studied here, two (Complexe Terminal) and (Continental Intercalaire)  
375 are the main aquifers of Sahara, by the extent (thousands of km from the recharge area to the Gulf  
376 of Gabès) and time of transfer (thousands of years). The last one, Phreatic aquifer, is shallow.  
377 The chemical facies have long been qualitatively described. Our results explain for the first  
378 time quantitatively the processes that occur during upward leakage through interaction between  
379 solution and the mineral constituents of the aquifers, and ultimately by mixing with surface  
380 waters.

381 The hydrochemical study of the aquifer system occurring in Ouargla's basin allowed us to  
382 identify the origin of its mineralization. Waters exhibit two different facies: sodium chloride and  
383 sodium sulfate for the phreatic aquifer (Phr), sodium sulfate for the Complexe Terminal (CT)  
384 aquifer and sodium chloride for the Continental Intercalaire (CI) aquifer. Calcium carbonate  
385 precipitation and evaporite dissolution explain the facies change from carbonate to sodium chlo-  
386 ride or sodium sulfate. However reactions imply many minerals with common ions, deep reac-  
387 tions without evaporation as well as shallow processes affected by both evaporation and mixing.  
388 Those processes are separated by considering both chemical and isotopic data, and quantitatively  
389 explained making use of an inverse geochemical modeling. The main result is that Phr waters  
390 do not originate simply from infiltration of rainwater and dissolution of salts from the sebkhas.  
391 Conversely, Phr waters are largely influenced by the upwardly mobile deep CT and CI groundwa-  
392 ters, fractions of the latter interacting with evaporites from Turonian formations. Phreatic waters  
393 occurrence is explained as a mixing of two end-member components: cluster I, which is very  
394 close to CI and CT, and cluster II, which is highly mineralized and results from the dissolution  
395 by rainwater of salts from the sebkhas.

396 At depth, CI leaks upwardly and dissolves gypsum, halite and sylvite, with some ion ex-  
397 change, to give waters of CT aquifer composition. CT transformation into Phr cluster I waters  
398 involves the dissolution of Turonian evaporites (halite, sylvite and bloedite) with minor calcite  
399 precipitation.

400 At the surface, direct dissolution by rainwater of salts from sebkhas (halite, sylvite, gypsum  
401 and some huntite) with precipitation of calcite and  $\text{Mg}^{2+}/\text{K}^{+}$  ion exchange results in cluster II  
402 Phr composition.

403 All phreatic groundwaters result from a mixing of cluster I and cluster II water that is accom-  
404 panied by calcite precipitation, fixation of  $\text{Mg}^{2+}$  on ion exchange sites against the release of  $\text{K}^{+}$   
405 and  $\text{Na}^{+}$ .

406 Moreover, some  $\text{CO}_{2(\text{g})}$  escapes from the solution at depth, but dissolves much more at the  
407 surface. The most complex phenomena occur during the dissolution of Turonian evaporites while  
408 CI leaks upwardly towards CT, and from Phr I to Phr II, while the transition from CT to Phr I

409 implies a very limited number of phases. Globally, gypsum dissolution and calcite precipitation  
 410 processes both act as an inorganic carbon sink.

#### 411 ACKNOWLEDGEMENTS

412 The authors wish to thank the staff members of the National Agency for Water Resources  
 413 in Ouargla (ANRH) and the Laboratory of Algerian Waters (ADE) for the support provided to  
 414 the Technical Cooperation programme within which this work was carried out. Analyses of  
 415  $^{18}\text{O}$  were funded by the project CDTN / DDHI (Guendouz and Moulla, 1996). The supports of  
 416 University of Ouargla and of INRA for travel grants of R. Slimani and G. Bourrié are gratefully  
 417 acknowledged too.

#### 418 APPENDIX

419 According to a simple Rayleigh equation, the evolution of the heavy isotope ratio in the  
 420 remaining liquid  $R_l$  is given by:

$$R_l \approx R_{l,0} \times f_l^{\alpha-1}, \quad (4)$$

421 where  $f_l$  is the fraction remaining liquid and  $\alpha$  the fractionation factor.

422 The fraction remaining liquid is derived from chloride concentration, as chloride can be con-  
 423 sidered as conservative during evaporation: all phreatic waters are undersaturated with respect to  
 424 halite, that precipitates only in the last stage. Hence, the following equation holds:

$$f_l \equiv \frac{n_{w,1}}{n_{w,0}} = \frac{[\text{Cl}^-]_0}{[\text{Cl}^-]_1}. \quad (5)$$

425 By taking natural logarithms, one obtains:

$$\ln R_l \approx (1 - \alpha) \times \ln[\text{Cl}^-] + \text{constant}, \quad (6)$$

426 As, by definition,

$$R_l \equiv R_{std.} \times \left(1 + \frac{\delta^{18}\text{O}}{1000}\right), \quad (7)$$

427 one has:

$$\ln R_l \equiv \ln R_{std.} + \ln\left(1 + \frac{\delta^{18}\text{O}}{1000}\right), \quad (8)$$

$$\approx \ln R_{std.} + \frac{\delta^{18}\text{O}}{1000}, \quad (9)$$

428 hence, with base 10 logarithms:

$$\delta^{18}\text{O} \approx 1000(1 - \alpha) \log[\text{Cl}^-] + \text{constant}, \quad (10)$$

$$\approx -\epsilon \log[\text{Cl}^-] + k, \quad (11)$$

429 where as classically defined  $\epsilon = 1000(\alpha - 1)$  is the enrichment factor.

430 **References**

- 431 Al-Gamal, S.A., 2011. An assessment of recharge possibility to North-Western Sahara Aquifer System (NWSAS) using  
 432 environmental isotopes. *Journal of Hydrology* 398, 184 – 190.
- 433 ANRH, 2011. Inventaire des forages de la Wilaya de Ouargla. Rapport technique. Agence Nationale des Ressources  
 434 Hydrauliques.
- 435 Aumassip, G., Dagorne, A., Estorges, P., Lefèvre-Witier, P., Mahrour, F., Nesson, C., Rouvillois-Brigol, M., Trecolle, G.,  
 436 1972. Aperçus sur l'évolution du paysage quaternaire et le peuplement de la région de Ouargla. *Libyca*, 205–257.
- 437 Belkhir, L., Boudoukha, A., Mouni, L., Baouz, T., 2010. Application of multivariate statistical methods and inverse  
 438 geochemical modeling for characterization of groundwater — A case study: Ain Azel plain (Algeria). *Geoderma*  
 439 159, 390 – 398.
- 440 Belkhir, L., Mouni, L., Boudoukha, A., 2012. Geochemical evolution of groundwater in an alluvial aquifer: Case of El  
 441 Eulma aquifer, East Algeria. *Journal of African Earth Sciences* 66–67, 46 – 55.
- 442 Carucci, V., Petitta, M., Aravena, R., 2012. Interaction between shallow and deep aquifers in the Tivoli Plain (Central  
 443 Italy) enhanced by groundwater extraction: A multi-isotope approach and geochemical modeling. *Applied Geochem-*  
 444 *istry* 27, 266 – 280. URL: <http://www.sciencedirect.com/science/article/pii/S0883292711004628>,  
 445 doi:<http://dx.doi.org/10.1016/j.apgeochem.2011.11.007>.
- 446 Chellat, S., Bourefis, A., Hamdi-Aïss, a.B., Djerrab, A., 2014. Paléoenvironnemental reconstitution of Mio-pliocenes  
 447 sandstones of the lower-Sahara at the base of exoscopic and sequential analysis. *Pensee Journal* 76, 34 – 51.
- 448 Chkir, N., Guendouz, A., Zouari, K., Hadj Ammar, F., Moulla, A., 2009. Uranium isotopes in groundwater from the  
 449 continental intercalaire aquifer in Algerian Tunisian Sahara (Northern Africa). *Journal of Environmental Radioac-*  
 450 *tivity* 100, 649 – 656. URL: <http://www.sciencedirect.com/science/article/pii/S0265931X09001143>,  
 451 doi:<http://dx.doi.org/10.1016/j.jenvrad.2009.05.009>.
- 452 Cornet, A., Gouscov, N., 1952. Les eaux du Crétacé inférieur continental dans le Sahara algérien: nappe dite "Albien",  
 453 in: *Congrès géologique international, Alger*. p. 30.
- 454 Dai, Z., Samper, J., Ritzi, R., 2006. Identifying geochemical processes by inverse modeling of multicomponent reactive  
 455 transport in the aquia aquifer. *Geosphere* 2, 210–219.
- 456 Deutsch, W., 1997. *Groundwater Chemistry-Fundamentals and Applications to Contamination*. New York.
- 457 Dubief, J., 1953. Essai sur l'hydrologie superficielle au Sahara. Direction du service de la colonisation et de  
 458 l'hydraulique, Service des études scientifiques.
- 459 Dubief, J., 1963. *Le climat du Sahara*. Hors-série, Institut de recherches sahariennes.
- 460 Eckstein, G., Eckstein, Y., 2003. A hydrogeological approach to transboundary ground water resources and international  
 461 law. *American University International Law Review* 19, 201–258.
- 462 Edmunds, W., Guendouz, A., Mamou, A., Moulla, A., Shand, P., Zouari, K., 2003. Groundwater evolution in the  
 463 continental intercalaire aquifer of southern Algeria and Tunisia: trace element and isotopic indicators. *Applied*  
 464 *Geochemistry* 18, 805–822.
- 465 Fontes, J., Yousfi, M., Allison, G., 1986. Estimation of long-term, diffuse groundwater discharge in the northern sahara  
 466 using stable isotope profiles in soil water. *Journal of Hydrology* 86, 315 – 327.
- 467 Foster, S., Margat, J., Droubi, A., 2006. Concept and importance of nonrenewable resources. Number 10 in IHP-VI  
 468 Series on Groundwater, UNESCO.
- 469 Furon, R., 1960. *Géologie de l'Afrique*. 2eme édition, Payot.
- 470 Güler, C., Thyne, G., 2004. Hydrologic and geologic factors controlling surface and groundwater chemistry in Indian  
 471 wells–Owens valley area, southeastern California, USA. *Journal of Hydrology* 285, 177–198.
- 472 Gonfiantini, R., Conrad, G., Fontes, J.C., Sauzay, G., Payne, B., 1975. Étude isotopique de la nappe du Continental  
 473 Intercalaire et de ses relations avec les autres nappes du Sahara septentrional. *Isotope Techniques in Groundwater*  
 474 *Hydrology* 1, 227–241.
- 475 Guendouz, A., 1985. Contribution à l'étude hydrochimique et isotopique des nappes profondes du Sahara nord-est  
 476 septentrional, Algérie. Phd thesis. Université d'Orsay, France.
- 477 Guendouz, A., Michelot, J., 2006. Chlorine-36 dating of deep groundwater from northern Sahara. *Journal of Hydrology*  
 478 328, 572–580.
- 479 Guendouz, A., Moulla, A., 1996. Étude hydrochimique et isotopique des eaux souterraines de la cuvette de Ouargla,  
 480 Algérie. Rapport technique. CDTN/DDHI.
- 481 Guendouz, A., Moulla, A., Edmunds, W., Zouari, K., Shands, P., Mamou, A., 2003. Hydrogeochemical and isotopic  
 482 evolution of water in the complex terminal aquifer in Algerian Sahara. *Hydrogeology Journal* 11, 483–495.
- 483 Hadj-Ammar, F., Chkir, N., Zouari, K., Hamelin, B., Deschamps, P., Aigoun, A., 2014. Hydro-  
 484 geochemical processes in the Complexe Terminal aquifer of southern Tunisia: An integrated investi-  
 485 gation based on geochemical and multivariate statistical methods. *Journal of African Earth Sciences*  
 486 100, 81 – 95. URL: <http://www.sciencedirect.com/science/article/pii/S1464343X14001940>,  
 487 doi:<http://dx.doi.org/10.1016/j.jafrearsci.2014.06.015>.

- 488 Hamdi-Aïssa, B., Vallès, V., Aventurier, A., Ribolzi, O., 2004. Soils and brines geochemistry and mineralogy of hyper  
489 arid desert playa, Ouargla basin, Algerian Sahara. *Arid Land Research and Management* 18, 103–126.
- 490 Kenoyer, G., Bowser, C., 1992. Groundwater chemical evolution in a sandy aquifer in northern Wisconsin. *Water*  
491 *Resources Research* 28, 591–600.
- 492 Kuells, C., Adar, E., Udluft, P., 2000. Resolving patterns of ground water flow by inverse hydrochemical modeling in a  
493 semiarid Kalahari basin. *Tracers and Modelling in Hydrogeology* 262, 447–451.
- 494 Le Houérou, H., 2009. *Bioclimatology and biogeography of Africa*. Springer Verlag.
- 495 Lelièvre, R., 1969. Assainissement de la cuvette de Ouargla. rapports Géohydraulique n° 2. Ministère des Travaux  
496 Publiques et de la construction.
- 497 Li, P., Qian, H., Wu, J., Ding, J., 2010. Geochemical modeling of groundwater in southern plain area of Pengyang  
498 County, Ningxia, China. *Water Science and Engineering* 3, 282–291.
- 499 Ma, J., Pan, F., Chen, L., Edmunds, W., Ding, Z., Zhou, K., He, J., Zhou, K., Huang, T., 2010. Isotopic and geochemical  
500 evidence of recharge sources and water quality in the Quaternary aquifer beneath Jinchang city, NW China. *Applied*  
501 *Geochemistry* 25, 996–1007.
- 502 Martinelli, G., Chahoud, A., Dadomo, A., Fava, A., 2014. Isotopic features of emilia-romagna region  
503 (north italy) groundwaters: Environmental and climatological implications. *Journal of Hydrology* 519, Part  
504 B, 1928 – 1938. URL: <http://www.sciencedirect.com/science/article/pii/S0022169414007690>,  
505 doi:<http://dx.doi.org/10.1016/j.jhydrol.2014.09.077>.
- 506 Matiatos, I., Alexopoulos, A., Godelitsas, A., 2014. Multivariate statistical analysis of the hydrogeochemical and isotopic  
507 composition of the groundwater resources in northeastern Peloponnesus (Greece). *Science of The Total Environment*  
508 476–477, 577 – 590. URL: <http://www.sciencedirect.com/science/article/pii/S0048969714000515>,  
509 doi:<http://dx.doi.org/10.1016/j.scitotenv.2014.01.042>.
- 510 Moulias, D., 1927. L'eau dans les oasis sahariennes, organisation hydraulique, régime juridique. Phd thesis. Alger.
- 511 Moulla, A., Guendouz, A., Cherchali, M.H., Chaid, Z., Ouarezki, S., 2012. Updated geochemical and isotopic data  
512 from the Continental Intercalaire aquifer in the Great Occidental Erg sub-basin (south-western Algeria). *Quaternary*  
513 *International* 257, 64–73.
- 514 OECD, 2008. *OECD Environmental Outlook to 2030. Technical Report 1*. Organisation for Economic Cooperation and  
515 Development.
- 516 ONM, 1975/2013. *Bulletins mensuels de relevé des paramètres climatologiques en Algérie*. Office national  
517 météorologique.
- 518 OSS, 2003. *Système aquifère du Sahara septentrional*. Technical Report. Observatoire du Sahara et du Sahel.
- 519 OSS, 2008. *Système aquifère du Sahara septentrional (Algérie, Tunisie, Libye): gestion concertée d'un bassin trans-*  
520 *frontalier*. Technical Report 1. Observatoire du Sahara et du Sahel.
- 521 Ould Baba Sy, M., Besbes, M., 2006. Holocene recharge and present recharge of the Saharan aquifers — a study by  
522 numerical modeling, in: *International symposium - Management of major aquifers*.
- 523 Parkhurst, D., Appelo, C., 2013. Description of Input and Examples for PHREEQC (Version 3) — A computer program  
524 for speciation, batch-reaction, one-dimensional transport, and inverse geochemical calculations. Technical Report 6.  
525 U.S. Department of the Interior, U.S. Geological Survey. URL: <http://pubs.usgs.gov/tm/06/a43>.
- 526 Plummer, L., Back, M., 1980. The mass balance approach: application to interpreting the chemical evolution of hydro-  
527 logical systems. *American Journal of Science* 280, 130–142.
- 528 Plummer, L., Sprinkle, C., 2001. Radiocarbon dating of dissolved inorganic carbon in groundwater from confined parts  
529 of the upper Floridan aquifer, Florida, USA. *Journal of Hydrology* 9, 127–150.
- 530 Sharif, M., Davis, R., Steele, K., Kim, B., Kresse, T., Fazio, J., 2008. Inverse geochemical modeling of groundwater  
531 evolution with emphasis on arsenic in the Mississippi River Valley alluvial aquifer, Arkansas (USA). *Journal of Hy-*  
532 *drology* 350, 41 – 55. URL: <http://www.sciencedirect.com/science/article/pii/S0022169407007093>,  
533 doi:<http://dx.doi.org/10.1016/j.jhydrol.2007.11.027>.
- 534 Slimani, R., 2006. Contribution à l'évaluation d'indicateurs de pollution environnementaux dans la région de Ouargla:  
535 cas des eaux de rejets agricoles et urbaines. Master's thesis. Université de Ouargla.
- 536 Stumm, W., Morgan, J., 1999. *Aquatic Chemistry: Chemical Equilibria and Rates in Natural Waters*. John Wiley and  
537 Sons.
- 538 Thomas, J., Welch, A., Preissler, A., 1989. Geochemical evolution of ground water in smith creek valley - a hydrologi-  
539 cally closed basin in central Nevada, USA. *Applied Geochemistry* 4, 493–510.
- 540 UNESCO, 1972. *Projet ERESS, Étude des ressources en eau du Sahara septentrional*. Technical Report 10. UNESCO.
- 541 Vallès, V., Rezagui, M., Auque, L., Semadi, A., Roger, L., Zouggari, H., 1997. Geochemistry of saline soils in two arid  
542 zones of the Mediterranean basin. I. Geochemistry of the Chott Melghir-Mehrouane watershed in Algeria. *Arid Soil*  
543 *Research and Rehabilitation* 11, 71–84.

Table 1: Field and analytical data for the Continental Intercalaire aquifer.

Locality	Lat.	Long.	Elev.	Date	EC	T	pH	Alk.	Cl <sup>-</sup>	SO <sub>4</sub> <sup>2-</sup>	Na <sup>+</sup>	K <sup>+</sup>	Mg <sup>2+</sup>	Ca <sup>2+</sup>	Br <sup>-</sup>
	/m														
Hedeb I	3,534,750	723,986	134	09/11/2012	2.0	46.5	7.6	3.5	5.8	6.8	10.7	0.6	2.5	3.3	0.034
Hedeb I	3,534,750	723,986	134	1992	1.9	49.3	7.3	0.4	5.8	1.1	5.7	0.2	0.8	0.5	
Hadeb II	3,534,310	724,290	146	1992	2.0	47.4	7.6	0.6	6.2	1.2	5.1	0.2	1.3	0.8	
Aouinet Moussa	3,548,896	721,076	132	1992	2.2	48.9	7.5	1.3	6.5	1.9	5.6	0.2	1.1	1.2	
Aouinet Moussa	3,548,896	721,076	132	22/02/2013	2.2	48.9	7.5	3.2	9.8	3.9	6.3	0.7	5.7	1.3	
Hedeb I	3,534,750	723,986	134	11/12/2010	2.2	49.3	7.3	1.9	12.4	4.6	10.7	0.7	3.8	2.3	
Hadeb II	3,534,310	724,290	146	11/12/2010	2.2	47.4	7.6	2.1	13.1	5.5	13.9	0.5	4.5	1.4	
Hassi Khelif	3,591,659	721,636	110	24/02/2013	2.4	50.5	6.8	2.9	14.3	5.2	10.8	0.8	3.4	4.6	0.033
Hedeb I	3,534,750	723,986	134	27/02/2013	2.0	46.5	7.6	3.5	15.1	7.7	11.8	0.5	5.6	5.2	
Hassi Khelif	3,591,659	721,636	110	09/11/2012	2.2	50.1	7.6	3.3	15.3	7.8	12.2	0.6	5.8	4.9	
El-Bour	3,560,264	720,366	160	22/02/2013	2.9	54.5	7.3	2.6	18.6	6.2	20.6	0.7	4.8	1.4	

Table 2: Field and analytical data for the Complexe Terminal aquifer.

Locality	Site	Aquifer	Lat.	Long.	Elev.	Date	EC	T	pH	Alk.	Cl <sup>-</sup>	SO <sub>4</sub> <sup>2-</sup>	Na <sup>+</sup>	K <sup>+</sup>	Mg <sup>2+</sup>	Ca <sup>2+</sup>	Br <sup>-</sup>
			/m														
Bamendil	D7F4	M	3,560,759	720,586	296	20/01/2013	2.0	20.1	7.9	1.6	10.1	5.8	9.9	0.7	3.9	2.5	
Bamendil	D7F4	M	3,560,759	720,586	296	1992	2.0	21.1	8.2	0.9	10.6	3.5	10.6	0.1	2.3	1.8	
Irfi	D1F151	S	3,538,891	721,060	204	1992	2.7	23.5	7.0	1.3	10.7	2.7	8.0	0.7	2.3	2.1	
Said Otha	D2F66	S	3,540,257	720,085	216	1992	2.3	24.0	8.0	1.4	11.0	4.7	11.5	0.2	2.1	3.3	
Oglat Larbaâ	D6F64	M	3,566,501	729,369	177	1992	2.3	18.0	7.9	1.4	11.4	6.8	11.6	2.3	2.0	4.6	
El-Bour	D4F94	M	3,536,245	722,641	100	27/01/2013	3.1	26.2	7.4	1.6	12.8	6.8	5.2	1.9	1.6	9.1	
Said Otha I	D2F71	S	3,557,412	718,272	211	1992	2.3	24.2	8.2	1.5	13.5	5.7	15.0	0.3	3.3	2.6	
Debieche	D6F61	M	3,547,557	717,067	173	26/01/2013	2.2	23.9	7.7	1.8	14.2	8.4	12.6	0.7	5.4	4.4	
Rouissat III	D3F10	S	3,535,068	722,352	248	1992	3.1	26.1	7.3	2.4	14.3	6.9	13.1	0.4	3.4	5.4	
Said Otha I	D2F71	S	3,557,412	718,272	212	26/01/2013	5.6	25.1	7.3	2.4	14.3	6.9	13.1	0.4	3.4	5.4	0.034
Rouissat III	D3F10	S	3,535,068	722,352	248	20/01/2013	2.3	18.9	8.0	1.6	15.2	8.6	12.6	1.6	5.8	4.3	
Irfi	D1F151	S	3,538,891	721,060	204	27/01/2013	2.4	22.9	7.8	1.7	15.4	8.3	13.7	0.2	5.2	4.8	
Said Otha	D2F66	S	3,540,257	720,085	216	31/01/2013	2.4	24.9	7.9	2.2	16.1	8.6	16.5	0.7	4.9	4.3	
Oglat Larbaâ	D6F64	M	3,566,501	729,369	177	31/01/2013	2.4	23.7	7.6	2.3	16.3	8.6	13.6	0.7	5.9	5.0	
SAR Mekhadma	D1F91	S	3,536,757	717,822	221	03/02/2013	2.5	25.8	7.7	3.4	16.5	8.5	16.1	0.7	5.3	4.9	
Sidi Kouiled	D9F12	S	3,540,855	729,055	329	24/01/2013	2.6	21.3	8.1	4.6	16.8	8.8	16.1	0.8	6.2	5.0	
Ain N'sara	D6F50	S	3,559,323	716,868	255	25/01/2013	3.4	25.7	7.4	2.0	16.9	9.7	15.9	0.3	3.4	7.9	0.033
A.Louise	D4F73	S	3,537,523	721,904	310	26/01/2013	2.6	24.0	7.5	2.0	17.4	9.1	13.9	2.0	5.8	5.1	
Ghazaleet A.H	D6F79	M	3,598,750	720,356	119	02/02/2013	2.8	22.5	7.5	3.5	17.4	9.3	16.6	0.6	6.2	4.9	
Ain moussa II	D9F30	S	3,537,814	719,665	220	02/02/2013	7.5	23.9	7.5	2.4	17.5	8.2	17.3	0.4	3.1	6.5	0.033
Ain N'sara	D6F50	S	3,559,323	716,868	255	02/02/2013	2.6	23.8	7.6	2.1	17.7	9.2	15.5	1.1	6.1	4.7	
H.Miloud	D1F135	M	3,547,557	717,067	173	03/02/2013	2.8	21.6	7.5	3.3	17.9	9.2	16.5	1.0	6.2	4.9	
El Bour	D6F97	S	3,540,936	715,816	169	25/01/2013	2.6	19.9	8.0	2.1	17.9	9.3	15.8	1.6	5.8	4.7	
H.Miloud	D1F135	M	3,547,557	717,067	173	1992	2.1	22.7	8.1	2.8	18.1	5.7	16.6	0.5	3.6	4.3	
N'goussa El Hou	D6F51	S	3,556,256	718,979	198	31/01/2013	2.9	22.9	7.5	2.0	18.4	9.6	17.1	0.5	6.2	5.0	
El Koum	D6F67	S	3,573,694	721,639	143	21/01/2013	3.1	22.9	8.1	3.5	18.4	9.7	17.9	0.3	6.5	5.1	
El Koum	D6F67	S	3,573,694	721,639	143	1992	2.5	25.0	7.6	1.5	18.8	7.2	10.2	3.4	5.0	5.8	
ITAS	D1F150	M	3,536,186	717,046	93	21/01/2013	3.7	23.9	7.5	1.5	18.8	7.1	10.1	3.4	5.0	5.8	
Ain moussa V	D9F13	M	3,538,409	718,680	210	08/02/2013	2.4	25.3	7.2	2.3	19.4	9.4	18.8	0.4	3.3	7.6	0.034
El-Bour	D4F94	M	3,536,245	722,641	100	1992	2.3	21.2	7.9	1.6	20.1	7.2	12.1	2.6	5.8	5.2	
Rouissat I	D3F18	M	3,535,564	722,498	80	26/01/2013	3.1	23.0	8.1	3.2	21.2	11.1	19.6	0.9	7.1	6.0	
Rouissat I	D3F18	M	3,535,564	722,498	80	1992	2.0	20.0	7.8	1.7	21.7	8.5	17.7	1.2	5.1	6.0	
St. pompage chott	D5F80	S	3,541,656	723,521	224	04/02/2013	3.3	24.5	8.2	3.9	22.1	11.9	19.9	2.1	7.6	6.3	
Chott Palmerate	D5F77	S	3,538,219	725,541	243	05/02/2013	3.4	24.6	7.5	3.3	22.3	12.1	20.9	1.2	8.3	5.8	
Bour El Haicha	D1F134	M	3,545,533	720,391	86	05/02/2013	3.4	22.2	7.3	4.1	23.2	12.2	21.2	1.5	8.6	6.0	
Abzart	D2F69	M	3,552,504	712,786	137	03/02/2013	3.5	24.6	7.6	2.2	24.7	12.7	21.1	1.7	8.5	6.5	
Garet Chemia	D1F113	S	3,536,174	716,808	213	28/01/2013	4.1	28.0	7.3	2.2	25.9	9.5	25.4	0.6	3.6	7.2	0.037
Frane	D6F62	M	3,570,175	717,133	167	27/01/2013	3.8	24.2	7.9	2.3	25.9	13.5	22.6	0.6	8.9	7.2	
Oum Raneb	D6 F69	M	3,540,451	721,919	216	25/01/2013	4.2	24.1	7.0	2.6	27.9	8.7	22.9	0.6	4.4	8.0	0.035
N'goussa El Hou	D6F51	S	3,556,256	718,979	198	1992	3.1	23.2	8.0	2.6	28.4	8.6	23.1	0.6	4.5	8.0	
H.Miloud Benyaza	D1F138	M	3,551,192	717,042	89	28/01/2013	3.8	25.2	7.6	2.4	28.4	14.2	23.9	1.7	10.0	7.1	
Ain Laarab	D6F49	M	3,558,822	716,799	156	28/01/2013	3.9	23.7	7.3	2.2	28.9	9.0	23.9	0.5	5.0	7.7	0.037
H.Miloud Benyaza	D1F138	M	3,551,192	717,042	89	1992	2.9	22.8	7.5	2.2	28.9	9.1	23.9	0.5	5.0	7.7	
Rouissat	D3F8	M	3,545,470	732,837	332	03/02/2013	4.4	25.4	7.5	1.7	29.8	8.3	22.8	1.2	6.2	6.1	
Rouissat	D3F8	M	3,545,470	732,837	332	1992	6.2	25.3	7.2	1.7	29.8	8.3	22.9	1.2	6.2	6.1	
Ain El Arch	D3F26	M	3,534,843	723,381	93	1992	5.1	25.1	7.4	1.6	34.7	8.9	24.0	0.9	8.4	6.5	
St. pompage chott	D5F80	S	3,541,656	723,521	224	1992	3.7	25.4	7.7	2.3	42.2	13.5	36.8	1.1	7.4	9.7	

M = Mio-pliocene aquifer; S = Senonian aquifer.



Table 4: Field and analytical data for the Phreatic aquifer (continued).

Locality	Site	Lat.	Long.	Elev.	Date	EC	T	pH	Alk.	Cl <sup>-</sup>	SO <sub>4</sub> <sup>2-</sup>	Na <sup>+</sup>	K <sup>+</sup>	Mg <sup>2+</sup>	Ca <sup>2+</sup>	Br <sup>-</sup>
		/m				/mS cm <sup>-1</sup> /°C	/mmol L <sup>-1</sup>									
Route Frane	P001	3,572,148	722,366	127	02/02/2013	66.2	28.3	7.2	6.5	468.7	101.5	350.3	26.0	116.2	35.3	
Sebkhet Safioune	P031	3,577,804	720,172	120	1992		23.8	7.3	6.3	481.8	43.4	326.8	12.6	94.2	23.6	
Sebkhet Safioune	P031	3,577,804	720,172	120	02/02/2013	76.0	27.9	8.1	5.9	500.3	110.3	470.5	28.7	79.1	35.5	
Route Frane	P002	3,570,523	722,028	108	1992		23.8	7.8	6.3	522.4	183.0	653.8	10.0	104.7	11.0	
Sebkhet Safioune	P030	3,577,253	721,936	130	1992		23.5	7.7	4.4	527.7	123.5	533.8	11.6	106.2	10.7	
Oum Raneb	P012	3,554,089	718,612	114	25/01/2013	64.1	30.3	7.8	7.8	534.3	20.9	529.6	6.4	19.7	4.7	
Oum Raneb	P012	3,554,089	718,612	114	1992		23.4	7.5	2.7	539.4	60.6	413.6	5.6	112.8	9.4	
ANK Djemel	P423	3,540,881	723,178	102	31/01/2013	90.8	23.5	7.5	6.2	636.5	101.3	495.5	38.3	125.8	30.3	
Said Otba-Chott	P096	3,540,265	724,729	111	1992		23.6	7.7	3.7	645.1	78.5	357.3	6.0	208.4	12.9	
Sebkhet Safioune	P030	3,577,253	721,936	130	03/02/2013	64.7	23.1	7.8	3.7	671.8	90.3	742.9	16.0	41.5	7.7	
N'Goussa	P017	3,560,256	715,781	130	26/01/2013	100.1	31.0	7.1	3.8	679.3	114.1	597.8	10.7	125.9	26.3	
ANK Djemel	P021	3,573,943	723,161	105	1992		23.6	7.4	4.2	700.8	154.5	605.7	53.6	163.1	14.2	
Station de pompage	PL04	3,541,410	723,501	138	1992		23.6	7.4	2.4	716.3	34.8	560.1	7.0	99.6	11.0	
Route Frane	P002	3,570,523	722,028	108	02/02/2013	62.8	26.9	7.6	1.7	748.5	62.6	651.5	14.7	77.7	27.3	
Said Otba-Chott	P096	3,540,265	724,729	111	03/02/2013	68.3	25.9	8.7	1.2	771.0	53.1	615.9	23.5	69.6	50.4	
N'Goussa	P019	3,562,960	717,719	113	1992		23.3	7.7	2.4	779.1	77.1	711.5	9.2	95.6	12.1	
Said Otba(Bab sbaa)	P066	3,542,636	718,957	126	03/02/2013	150.6	26.2	7.2	12.3	799.1	283.0	1,249.7	19.0	37.6	18.1	
ANK Djemel	P021	3,573,943	723,161	105	24/01/2013	82.3	29.6	7.6	2.4	800.4	94.4	824.0	11.0	53.4	25.4	
N'Goussa	P018	3,562,122	716,590	110	1992		23.3	7.5	1.2	818.7	81.0	244.2	49.5	319.4	24.8	
Oum Raneb	P162	3,546,133	725,129	98	25/01/2013	160.0	30.7	7.2	2.4	842.8	289.9	1,309.9	13.3	33.5	17.7	
Route Sedrata	P113	3,535,586	714,576	105	1992		23.7	7.7	2.8	954.9	124.9	997.5	13.3	86.7	11.7	
Oum Raneb	PZ12	3,547,234	722,931	110	05/02/2013	114.9	27.4	7.4	2.9	980.1	15.5	930.8	7.5	23.9	14.2	
Hôtel Transat	PL23	3,538,419	720,950	126	1992		23.5	7.4	3.0	1,103.3	94.5	707.8	19.1	270.9	13.3	
Sebkhet Safioune	P023	3,577,198	725,726	99	1992		23.3	7.4	2.3	1,177.0	91.1	1,058.2	11.7	133.5	12.4	
Sebkhet Safioune	P034	3,579,698	725,633	97	05/02/2013	130.0	34.9	8.1	1.8	1,189.1	14.7	1,055.1	18.3	56.4	17.4	
Sebkhet Safioune	P023	3,577,198	725,726	99	05/02/2013	117.9	29.4	8.2	1.9	1,209.3	15.6	1,129.4	8.4	42.9	10.2	
Chott Adjadja	PLX1	3,540,758	726,115	132	1992		23.6	8.0	3.8	1,296.7	134.0	1,458.7	5.2	48.0	4.3	
Sebkhet Safioune	P063	3,545,586	725,667	99	1992		23.5	7.5	1.9	1,379.4	139.6	1,257.4	18.6	182.3	10.0	
LTP06					1992		23.8	7.6	7.8	1,638.7	712.1	2,621.6	41.6	190.5	13.3	
Bamendil	P076	3,540,137	716,721	118	1992		23.5	7.7	5.7	1,743.6	143.4	1,321.9	26.9	331.4	12.3	
El Bour-N'gouca	P007	3,562,236	718,651	129	1992		23.3	7.7	1.4	1,860.5	91.6	1,434.7	26.2	278.8	13.3	
Sebkhet Safioune	P063	3,545,586	725,667	99	05/02/2013	178.9	26.7	7.7	1.4	1,887.9	92.9	1,455.8	26.7	282.9	13.4	
	P044				1992		23.4	7.8	4.5	2,106.1	18.3	1,765.5	27.3	171.2	6.5	
	P093				1992		23.6	7.5	1.5	2,198.6	182.1	1,957.5	29.5	278.2	10.4	
	P042				1992		23.4	7.6	1.1	2,330.9	101.2	1,963.7	52.2	248.1	11.2	
	P068				1992		23.5	7.5	3.4	2,335.7	222.1	2,302.3	26.8	219.9	7.2	
Oum Raneb	PZ12	3,547,234	722,931	110	1992		23.3	7.6	2.2	2,405.6	109.9	2,178.6	25.2	199.4	12.7	
Hassi Debich	P416	3,581,097	730,922	106	1992		23.3	7.8	4.3	2,433.7	178.9	2,361.1	24.3	196.1	9.2	
N'Goussa	P041	3,559,563	716,543	135	1992		23.4	7.9	2.1	2,599.7	324.6	2,879.0	44.6	152.8	11.0	
Sebkhet Safioune	P034	3,579,698	725,633	97	1992		23.3	7.8	1.9	2,752.0	134.1	2,616.8	24.4	180.1	10.5	
	P039				1992		23.4	6.9	1.9	4,189.5	201.4	4,042.6	17.9	257.8	9.2	
Sebkhet Safioune	P074				1992		23.5	6.5	4.2	4,356.5	180.9	2,759.9	57.4	930.1	22.6	
Sebkhet Safioune	P037				1992		23.4	6.9	1.5	4,953.8	184.5	4,611.1	2.9	347.6	7.9	
Sebkhet Safioune	P036				1992		23.4	7.5	1.4	4,972.8	108.1	4,692.2	36.8	221.1	9.6	

For longitude and latitude, the reference is UTM 31 projection for North Sahara 1959 (CLARKE 1880 ellipsoid).



Table 5: Isotopic data  $^{18}\text{O}$  and  $^3\text{H}$  and chloride concentration in Continental Intercalaire, Complexe Terminal and Phreatic aquifers (sampling campaign in 1992).

Phreatic aquifer											
Piezometer	$\text{Cl}^-$ /mmol L $^{-1}$	$\delta^{18}\text{O}$ /‰	$^3\text{H}$ /UT	Piezometer	$\text{Cl}^-$ /mmol L $^{-1}$	$\delta^{18}\text{O}$ /‰	$^3\text{H}$ /UT	Piezometer	$\text{Cl}^-$ /mmol L $^{-1}$	$\delta^{18}\text{O}$ /‰	$^3\text{H}$ /UT
P007	1.860.5	-2.5	0	PL15	23.5	-7.85	0.6(1)	P074	4.356.4	3.4	6.8(8)
P009	426.9	-6.6	1.2(3)	P066	80.2	-8.1	0.8(1)	PL06	14.2	-8.1	1.0(2)
P506	54.4	-6.8	1.6(3)	PL23	1,103.3	-6.1	0	PL30	24.3	-7.48	2.4(4)
P018	818.7	-2.9	6.2(11)	P063	1,379.3	-3.4	8.7(15)	P002	522.4	-5.7	0.6(1)
P019	779.1	-4.7	5.6(9)	P068	2,335.6	-3.1	8.8(14)	PL21	84.3	-7.7	1.2(2)
PZ12	2,405.5	-2.3	8.1(13)	P030	527.7	-6.6	2.4(4)	PL31	18.9	-7.4	1.6(3)
P023	1,176.9	-2.6	0.2(1)	P076	1,743.5	-5.6	2.8(5)	P433	12.0	-8.8	0
P416	2,433.7	-7.9	5.9(9)	P021	700.7	-5.2	2.6(4)	PL03	84.1	-7.4	1.7(3)
P034	2,752.0	-1.8	5.7(9)	PL04	716.3	-2.9		PL44	109.8	-8.8	1.0(2)
P036	4,972.7	3.3	2.1(4)	P093	2,198.5	-2.6	5.1(8)	PL05	30.9	-7.4	1.9(3)
P037	4,953.8	3.1	1.8(3)	P096	645.1	-6.1	4.8(8)	P408	24.2	-7.9	0
P039	4,189.5	1.0	2.2(4)	PLX1	1,296.6	-5.6	1.1(2)	P116	31.9	-7.2	1.1(2)
P041	2,599.7	-0.6	7.3(13)	PLX2	25.7	-7.6	1.3(2)	LTP 16	213.4	-7.5	1.6(3)
P044	2,106.1	-4.5	2.7(5)	P015	134.7	-6.8	3.0(5)	P117	32.8	-6.9	0.1
P014	336.9	-6.9	2.8(5)	P001	323.6	-4.7	2.5(4)	PL10	35.0	-7.3	0.2(1)
P012	539.3	-6.4	2.2(4)	P100	235.0	-5.8	0	PL25	75.6	-7.4	0.9(2)
P042	2,330.8	2.1	6.0(10)	P056	42.1	-7.0	2.9(5)	LTP30	18.2	-7.5	1.1(2)
P006	19.0	-6.6	0.5(1)	P113	954.9	-4.8	0.8(2)	LTP06	1,638.6	-1.9	2.8(5)
P057	28.2	-7.3	1.1(2)	PLX4	31.5	-7.1	0.3(1)	P031	481.8	-6.1	3.0(5)
P059	20.8	-7.8	0	P115	28.8	-2.5	6.8(12)				

Complexe Terminal aquifer											
Borehole	$\text{Cl}^-$ /mmol L $^{-1}$	$\delta^{18}\text{O}$ /‰	$^3\text{H}$ /UT	Borehole	$\text{Cl}^-$ /mmol L $^{-1}$	$\delta^{18}\text{O}$ /‰	$^3\text{H}$ /UT	Borehole	$\text{Cl}^-$ /mmol L $^{-1}$	$\delta^{18}\text{O}$ /‰	$^3\text{H}$ /UT
D5F80	42.2	-7.9		D1F138	28.9	-8.1	0.7(1)	D2F71	13.5	-8.2	0.6(1)
D3F8	29.8	-8.1	1.4(2)	D3F18	21.7	-8.2	0.2(1)	D7F4	10.6	-8.3	0.1(1)
D3F26	34.7	-8.0	0.8(1)	D3F10	14.3	-7.9	1.5(2)	D2F66	11.0	-8.3	
D4F94	20.1	-8.2	0.6(1)	D6F51	28.4	-7.9	0.7(1)	D1F151	10.8	-8.3	0.4(1)
D6F67	18.8	-8.2	3.7(6)	D1F135	18.1	-8.1	1.1(2)	D6F64	11.4	-8.3	4.3(7)

Continental Intercalaire aquifer											
Borehole	$\text{Cl}^-$ /mmol L $^{-1}$	$\delta^{18}\text{O}$ /‰	$^3\text{H}$ /UT	Borehole	$\text{Cl}^-$ /mmol L $^{-1}$	$\delta^{18}\text{O}$ /‰	$^3\text{H}$ /UT	Borehole	$\text{Cl}^-$ /mmol L $^{-1}$	$\delta^{18}\text{O}$ /‰	$^3\text{H}$ /UT
Hadeb I	5.8	-8.0	0	Hadeb II	6.2	-7.9	0.1(1)	Aouinet Moussa	6.5	-7.9	1.1(2)

Table 6: Statistical parameters for Continental Intercalaire (CI), Complexe Terminal (CT) and Phreatic (Phr) aquifers samples selected on the basis of  $\delta^{18}\text{O}$  and  $\text{Cl}^-$  data (see text).

Aquifer	Size	Parameter	EC /mS cm $^{-1}$	T /°C	pH	Alk.	$\text{Cl}^-$	$\text{SO}_4^{2-}$	$\text{Na}^+$	$\text{K}^+$	$\text{Mg}^{2+}$	$\text{Ca}^{2+}$
			/mmol/L									
CI	11	Average	2.2	49.0	7.5	2.3	11.0	4.7	10.3	0.5	3.6	2.4
CI	11	Stdd. dev.	0.3	2.0	0.2	1.0	4.6	2.5	4.6	0.2	2.0	1.8
CT	50	Average	3.2	23.0	7.8	2.3	20.0	8.9	17.0	1.0	5.5	5.6
CT	50	Stdd. dev.	1.1	2.4	0.4	0.8	7.0	2.6	6.0	0.8	2.2	1.7
Phr cluster I	30	Average	3.9	24.0	7.9	2.3	24.7	11.8	24.2	2.1	7.2	5.3
Phr cluster I	30	Stdd. dev.	1.3	1.3	0.4	1.0	6.9	3.4	11.0	1.7	5.0	2.7
Phr cluster II	3	Average		23.4	7.0	2.4	4,761.0	158.0	4,021.0	32.4	500.0	13.0
Phr cluster II	3	Stdd. dev.		0.1	0.5	1.6	350.0	43.0	1,093.0	28.0	378.0	8.0

Table 7: Summary of mass transfer for geochemical inverse modeling. Phases and thermodynamic database are from Phreeqc 3.0 (Parkhurst and Appelo, 2013).

Phases	Stoichiometry	CI/CT	CT/Phr I	Rainwater/P036	PhrI/PhrII 60%/40%
Calcite	CaCO <sub>3</sub>	—	$-6.62 \times 10^{-6}$	$-1.88 \times 10^{-1}$	$-2.26 \times 10^{-1}$
CO <sub>2</sub> (g)	CO <sub>2</sub>	$-6.88 \times 10^{-5}$	—	$8.42 \times 10^{-4}$	$5.77 \times 10^{-4}$
Gypsum	CaSO <sub>4</sub> · 2 H <sub>2</sub> O	$4.33 \times 10^{-3}$	—	$1.55 \times 10^{-1}$	$1.67 \times 10^{-1}$
Halite	NaCl	$7.05 \times 10^{-3}$	$3.76 \times 10^{-3}$	6.72	1.28
Sylvite	KCl	$2.18 \times 10^{-3}$	$1.08 \times 10^{-3}$	$4.02 \times 10^{-1}$	—
Bloedite	Na <sub>2</sub> Mg(SO <sub>4</sub> ) <sub>2</sub> · 4 H <sub>2</sub> O	—	$1.44 \times 10^{-3}$	—	—
Huntite	CaMg <sub>3</sub> (CO <sub>3</sub> ) <sub>4</sub>	—	—	$4.74 \times 10^{-2}$	$5.65 \times 10^{-2}$
Ca ion exchange	CaX <sub>2</sub>	$-1.11 \times 10^{-3}$	—	—	—
Mg ion exchange	MgX <sub>2</sub>	$1.96 \times 10^{-3}$	—	$1.75 \times 10^{-1}$	$-2.02 \times 10^{-1}$
Na ion exchange	NaX	—	—	—	$3.92 \times 10^{-1}$
K ion exchange	KX	$-1.69 \times 10^{-3}$	—	$-3.49 \times 10^{-1}$	$1.20 \times 10^{-2}$

Values are in mol/kg (H<sub>2</sub>O). Positive (mass entering solution) and negative (mass leaving solution) phase mole transfers indicate dissolution and precipitation, respectively; — indicates no mass transfer.

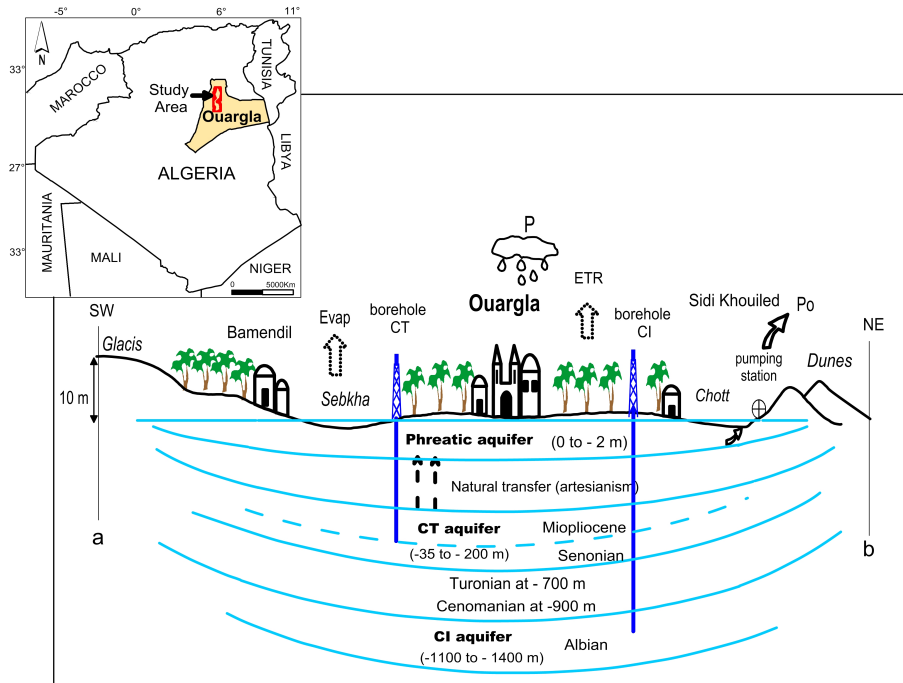


Figure 1: Location and schematic relations of aquifers in Ouargla. Blue lines represent limits between aquifers, and the names of aquifers are given in bold letters; as the limit between Senonian and Mio-pliocene aquifers is not well defined, a dashed blue line is used. Names of villages and cities are given in roman (Bamendil, Ouargla, Sidi Khouiled), while geological/geomorphological features are in italic (Glacis, Sebkhha, Chott, Dunes). Depths are relative to the ground surface. Letters a and b refer to the cross section (fig. 2) and to the localisation map (fig. 3).

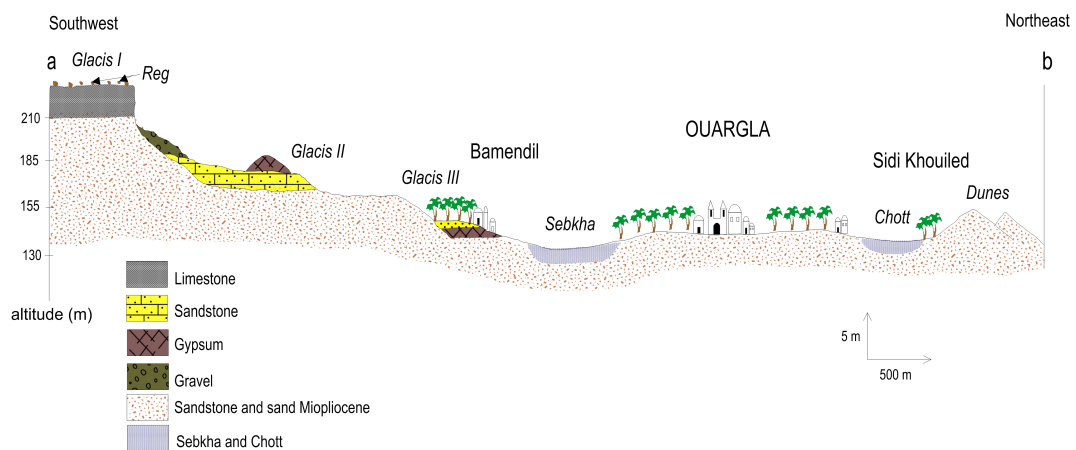


Figure 2: Geologic cross section in the region of Ouargla. The blue pattern used for Chott and Sebkhha correspond to the limit of the saturated zone.

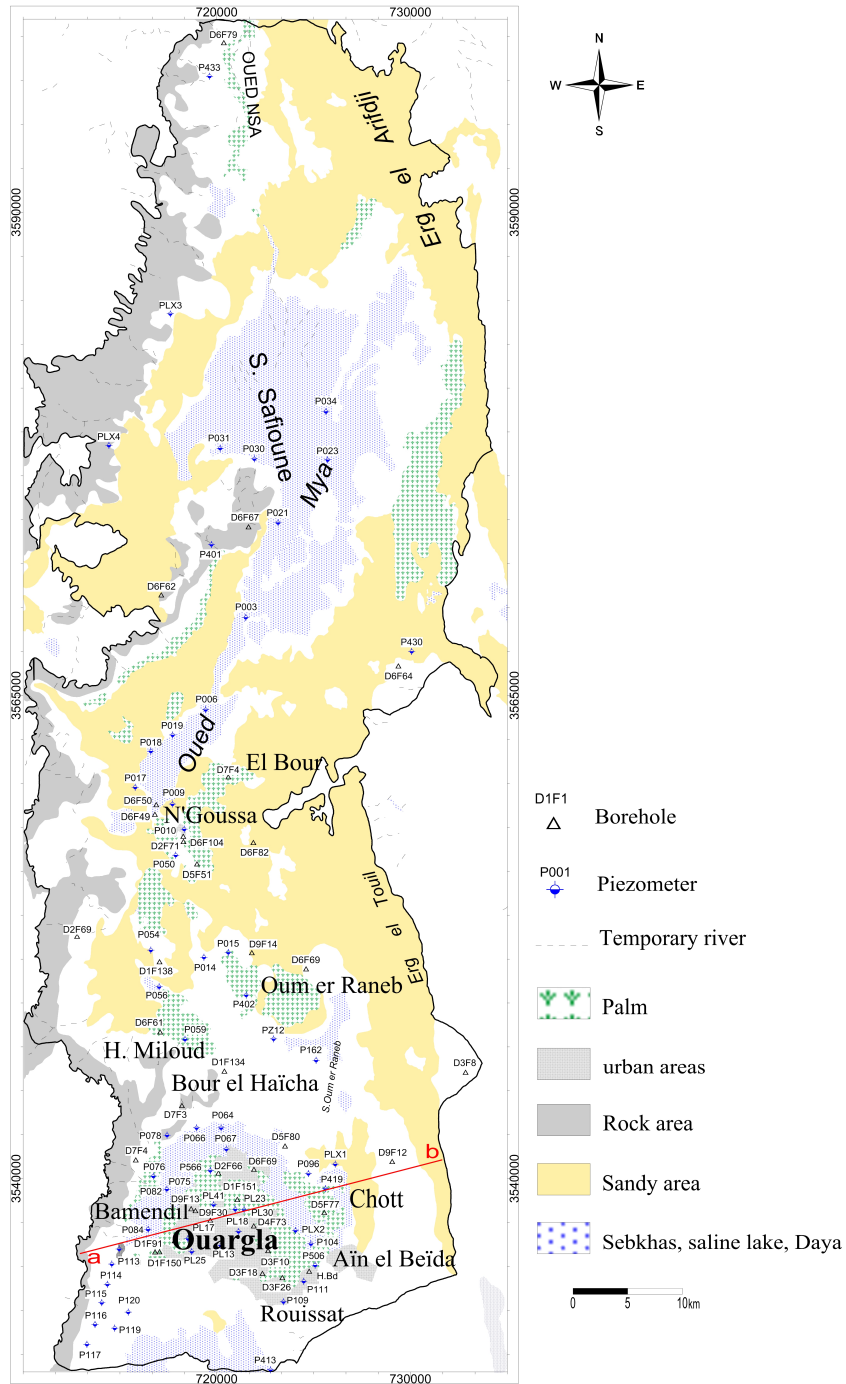


Figure 3: Location map of sampling points

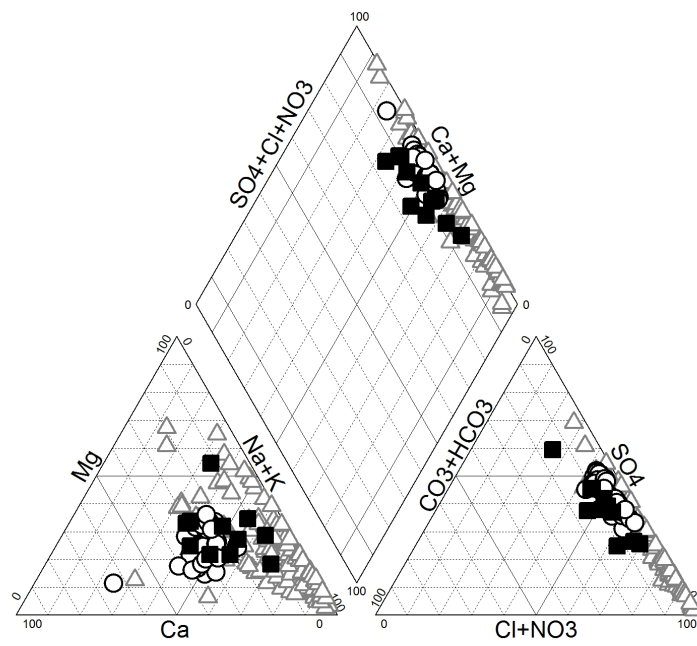
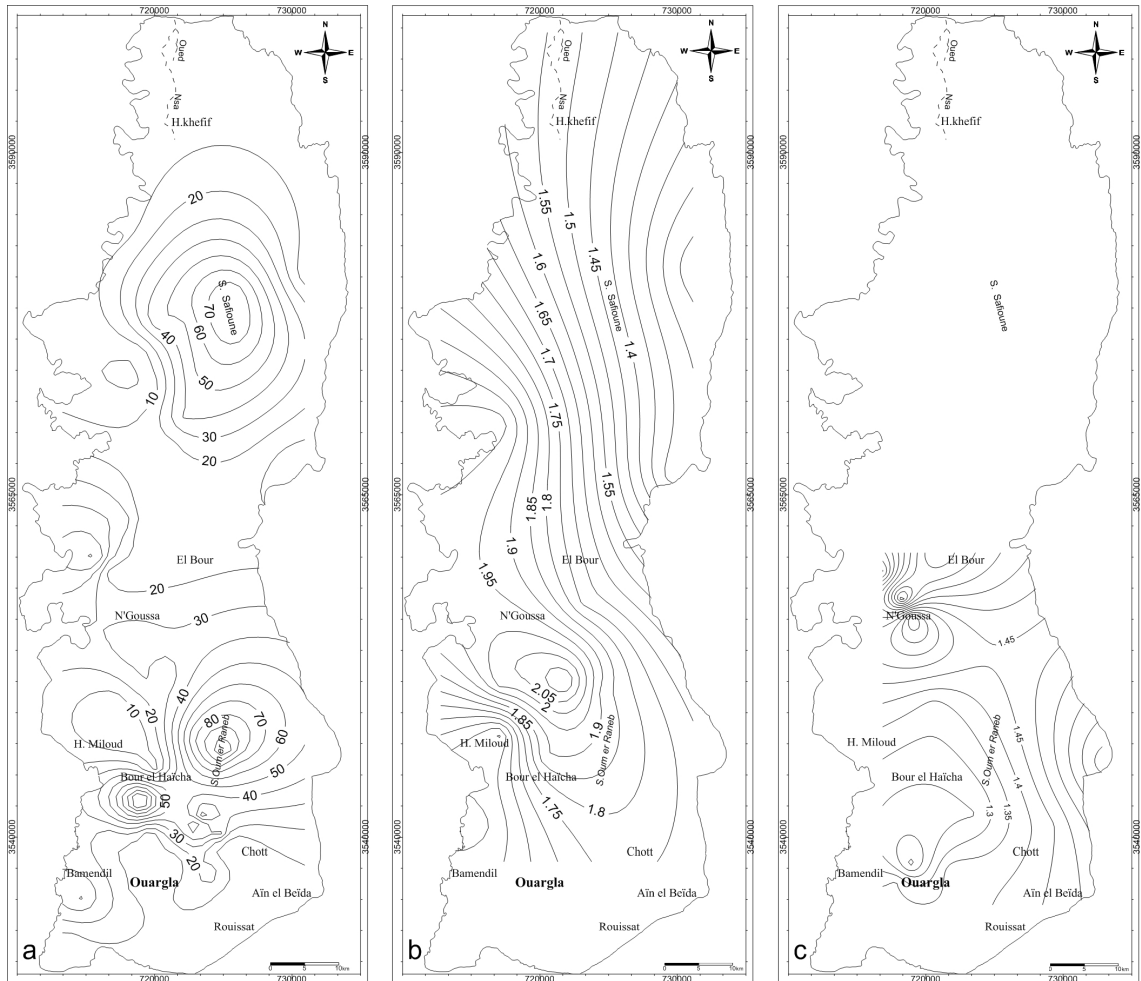


Figure 4: Piper diagram for Continental Intercalaire (filled squares), Complexe Terminal (open circles) and Phreatic aquifer (open triangles).



5

Figure 5: Contour maps of the salinity (expressed as global mineralization) in the aquifer system, (a) Phreatic aquifer; (b) and (c) Complex Terminal [(b) Mio-pliocene and (c) Senonian]; figures are isovalues of global mineralization (values in g/L).

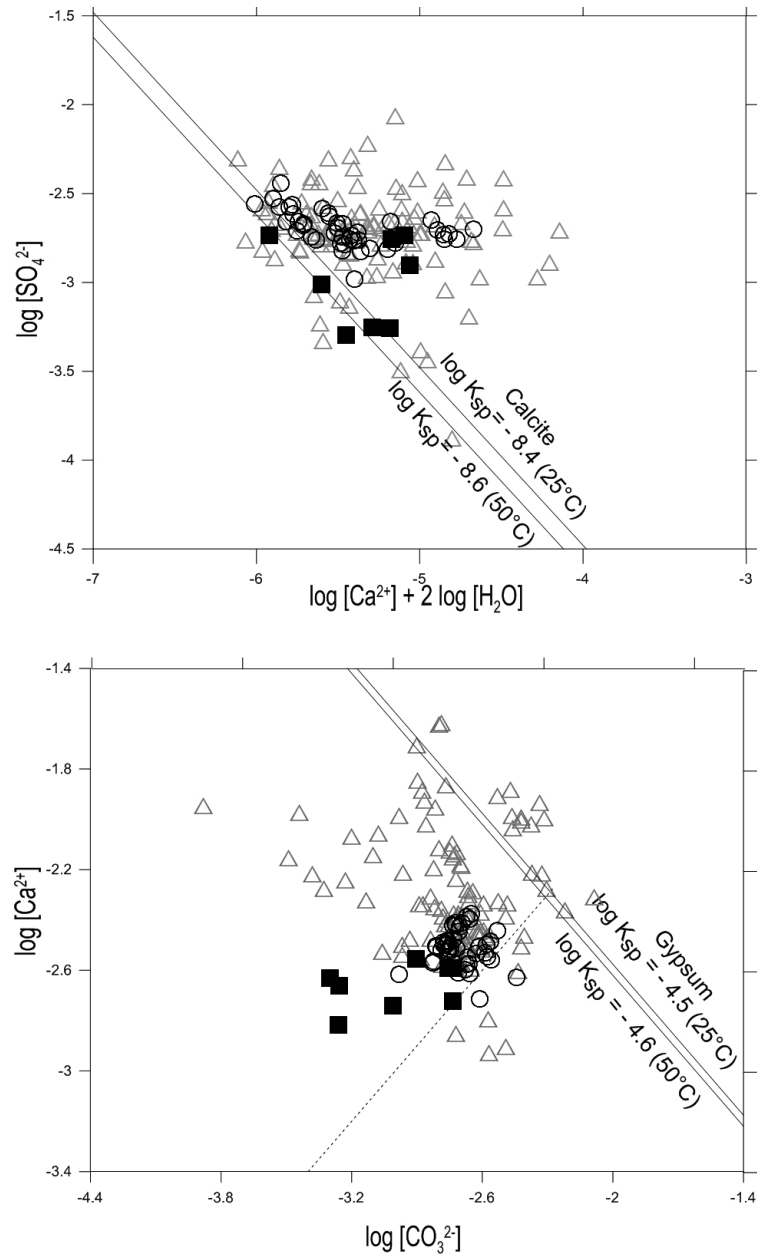


Figure 6: Equilibrium diagrams of calcite (top) and gypsum (bottom) for Continental Intercalaire (filled squares), Complexe Terminal (open circles) and Phreatic aquifer (open triangles). Equilibrium lines are defined as:  $\log[\text{Ca}^{2+}] + \log[\text{CO}_3^{2-}] = \log K_{sp}$  for calcite, and  $\log[\text{Ca}^{2+}] + 2 \log[\text{H}_2\text{O}] + \log[\text{SO}_4^{2-}] = \log K_{sp}$  for gypsum.

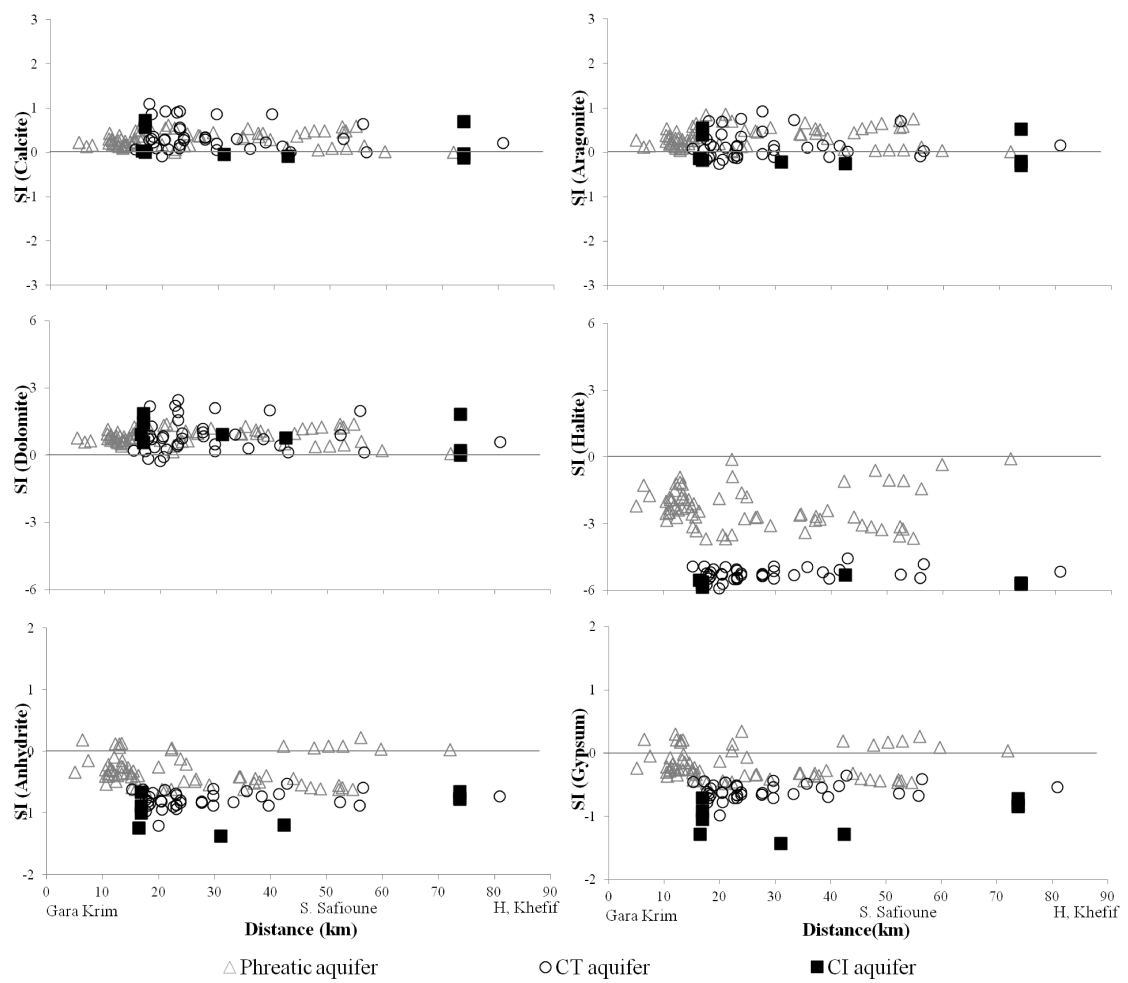


Figure 7: Variation of saturation indices with distance from south to north in the region of Ouargla.



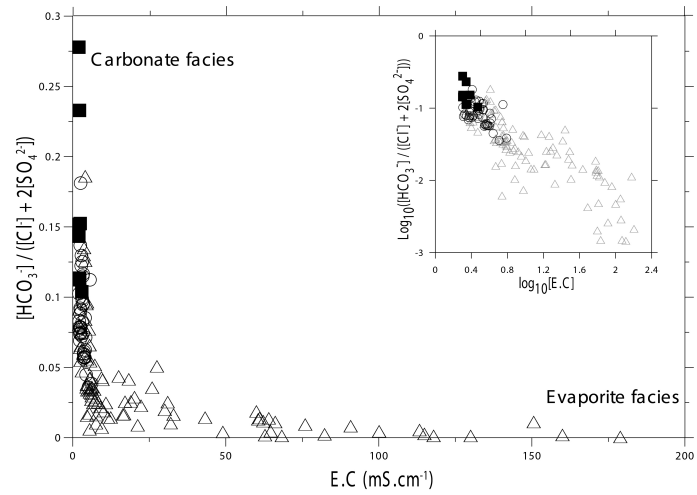


Figure 8: Change from carbonate facies to evaporite from Continental Intercalaire (filled squares), Complex Terminal (open circles) and Phreatic aquifer (open triangles).

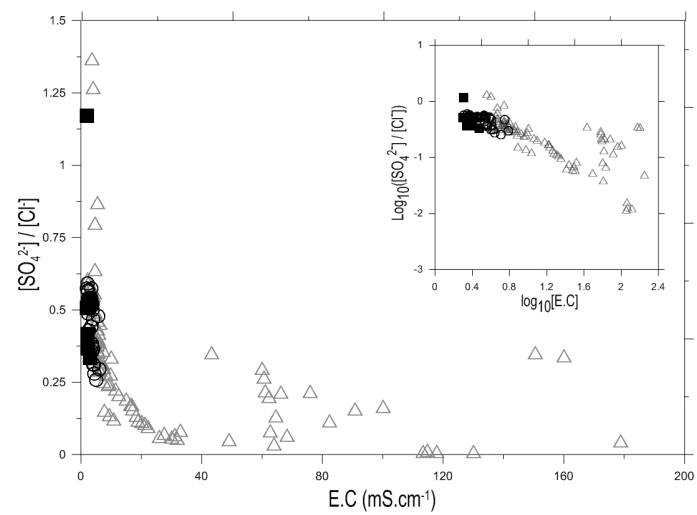


Figure 9: Change from sulfate facies to chloride from Continental Intercalaire (filled squares), Complex Terminal (open circles) and Phreatic aquifer (open triangles).

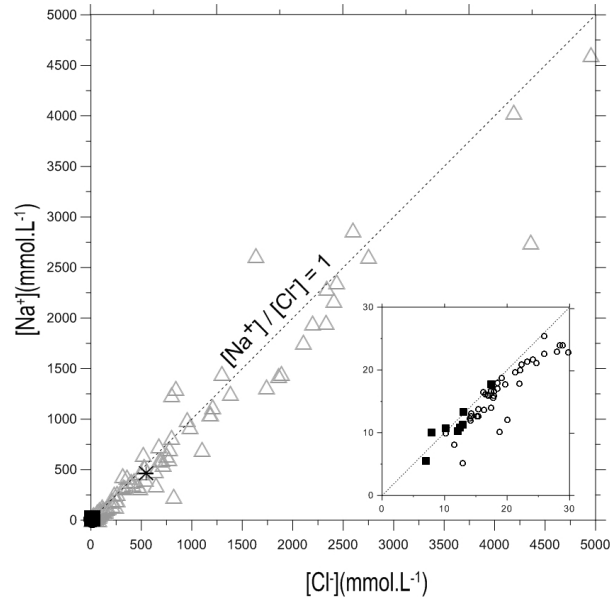


Figure 10: Correlation between  $Na^+$  and  $Cl^-$  concentrations in Continental Intercalaire (filled squares), Complex Terminal (open circles) and Phreatic aquifer (open triangles). Seawater composition (star) is  $[Na^+] = 459.3$  mmol.L<sup>-1</sup> and  $[Cl^-] = 535.3$  mmol.L<sup>-1</sup> (Stumm and Morgan, 1999, p.899).

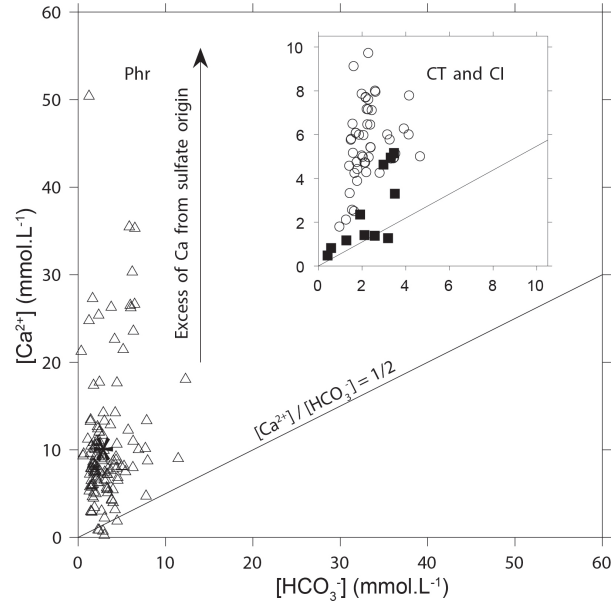


Figure 11: Calcium vs.  $HCO_3^-$  diagram in Continental Intercalaire (filled squares), Complex Terminal (open circles), Phreatic aquifer (open triangles) and Seawater composition (star) is  $[Ca^{2+}] = 10.2$  mmol.L<sup>-1</sup> and  $[HCO_3^-] = 2.38$  mmol.L<sup>-1</sup> (Stumm and Morgan, 1999, p.899).

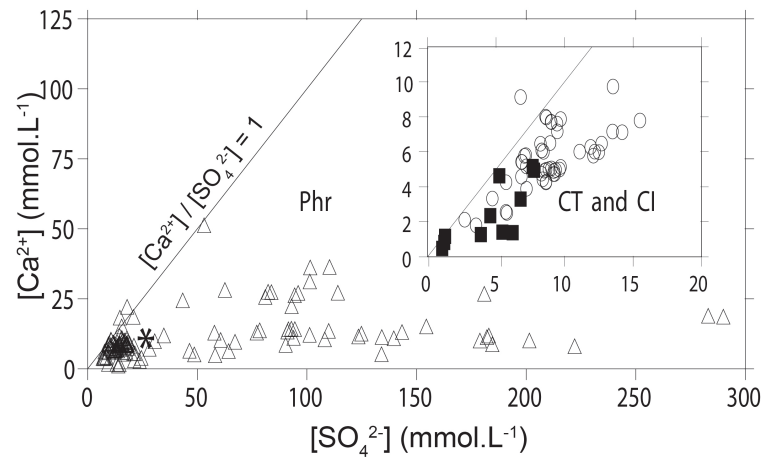


Figure 12: Calcium vs.  $\text{SO}_4^{2-}$  diagram in Continental Intercalaire (filled squares), Complexe Terminal (open circles), Phreatic aquifer (open triangles) and Seawater composition (star) is  $[\text{Ca}^{2+}] = 10.2 \text{ mmol L}^{-1}$  and  $[\text{SO}_4^{2-}] = 28.2 \text{ mmol L}^{-1}$  (Stumm and Morgan, 1999, p.899).

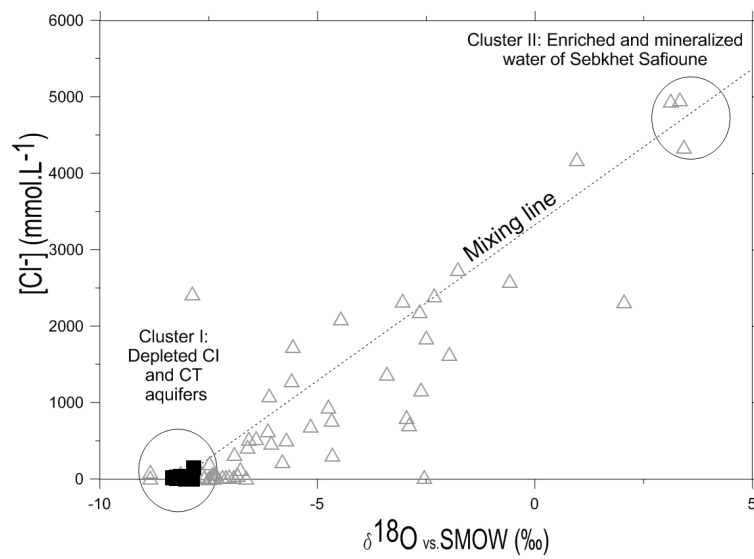


Figure 13: Chloride concentration versus  $\delta^{18}\text{O}$  in Continental Intercalaire (filled squares), Complexe Terminal (open circles) and Phreatic aquifer (open triangles) from Ouargla.

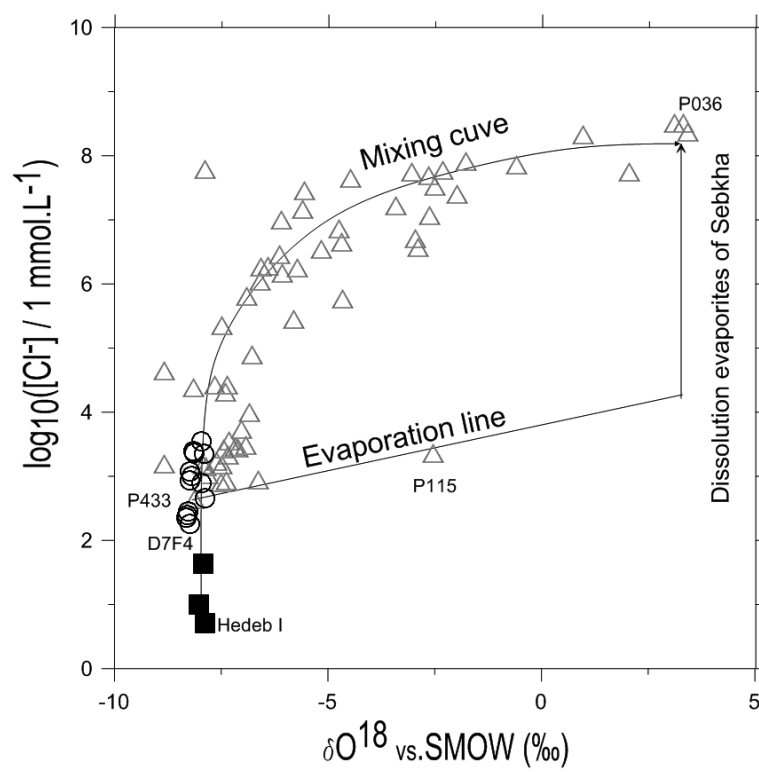


Figure 14: Log  $[\text{Cl}^-]$  concentration versus  $\delta^{18}\text{O}$  in Continental Intercalaire (filled squares), Complexe Terminal (open circles) and Phreatic aquifer (open triangles) from Ouargla.